AD-A096 980 BOLT BERANEK AND NEWMAN INC CAMBRIDGE MA F/G 17/8
LASER DOPPLER AIRSPEED AND ALTITUDE SENSOR.(U)
FEB 81 M J RUDD F49620-78-C-0023
UNCLASSIFIED AFOSR-TR-81-0309 NL

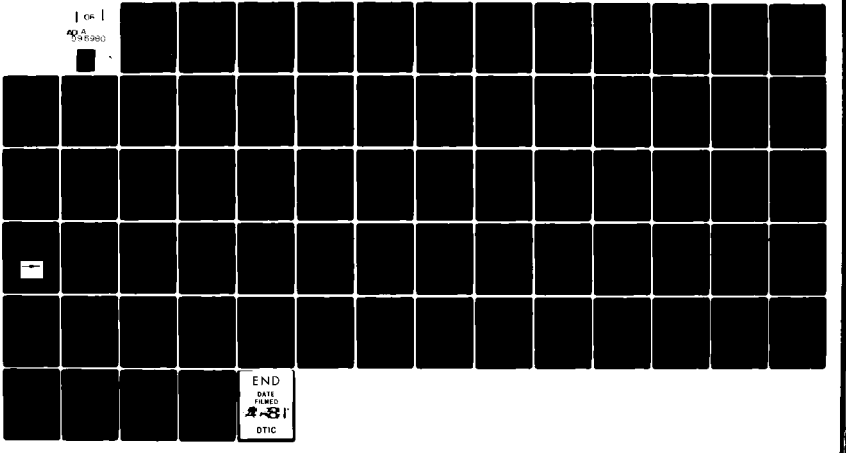

Bolt Beranek and Newman Inc.

Report No. 4607

Laser Doppler Airspeed and Altitude Sensor

Final Report

M.J. Rudd

February 1981

F49620-78-C-0023

Prepared for:
Air Force Office of Scientific Research

UNCLASSIFIED

SECURITY CLASSIFICATION OF THIS PAGE (When Data Entered)

REPORT DOCUMENTATION PAGE		READ INSTRUCTIONS BEFORE COMPLETING FORM
1. REPORT NUMBER AFOSR-TR- 81-0309	2. GOVT ACCESSION NO. AD-A096 980	3. RECIPIENT'S CATALOG NUMBER
4. TITLE (and Subtitle) Laser Doppler Airspeed and Altitude Sensor —		5. TYPE OF REPORT & PERIOD COVERED Final 10/15/77-11/15/80
		6. PERFORMING ORG. REPORT NUMBER 4607
7. AUTHOR(s) M.J. Rudd		8. CONTRACT OR GRANT NUMBER(s) F49620-78-C-0023
9. PERFORMING ORGANIZATION NAME AND ADDRESS Bolt Beranek and Newman Inc. 10 Moulton St., Cambridge, MA 02238		10. PROGRAM ELEMENT, PROJECT, TASK AREA & WORK UNIT NUMBERS 61102F 2305/B2
11. CONTROLLING OFFICE NAME AND ADDRESS Air Force Office of Scientific Research Bolling Air Force Base, Code NE Washington, DC 20332		12. REPORT DATE February 1981 13. NUMBER OF PAGES 70
14. MONITORING AGENCY NAME & ADDRESS(if different from Controlling Office)		15. SECURITY CLASS. (of this report) Unclassified 15a. DECLASSIFICATION/DOWNGRADING SCHEDULE

16. DISTRIBUTION STATEMENT (of this Report)

Approved for public release;
distribution unlimited.

17. DISTRIBUTION STATEMENT (of the abstract entered in Block 20, if different from Report)

18. SUPPLEMENTARY NOTES

19. KEY WORDS (Continue on reverse side if necessary and identify by block number)

Air Data System, Airspeed, Altitude, Laser, Infra-red Fluorescence, Carbon Dioxide, Correlation

20. ABSTRACT (Continue on reverse side if necessary and identify by block number)

The feasibility of an air data system based on the measurement of the resonant fluorescence of carbon dioxide in the atmosphere is discussed. The Doppler shift of the fluorescence gives the air velocity and the linewidth gives the pressure altitude.

A system using a tunable diode laser has been set-up and characterized. Attempts to measure back-scattered fluorescence were unsuccessful, but

DD FORM 1 JAN 73 1473 EDITION OF 1 NOV 65 IS OBSOLETE

UNCLASSIFIED

SECURITY CLASSIFICATION OF THIS PAGE (When Data Entered)

inelastic scattering in the forward direction was observed. Mechanisms for this are discussed but no firm conclusion is reached. A correlation technique for processing the data is discussed and its accuracy conputed.

Report No. 4607

LASER DOPPLER AIRSPEED AND ALTITUDE SENSOR

Final Report.

M.J. Rudd

February 1981

Prepared by:

Bolt Beranek and Newman Inc.
10 Moulton Street
Cambridge, MA 02238

Prepared for:

Air Force Office of Scientific Research
Bolling Air Force Base, Code NE
Washington, DC 20332

ABSTRACT

The feasibility of an air data system based on the measurement of the resonant fluorescence of carbon dioxide in the atmosphere is discussed. The Doppler shift of the fluorescence gives the air velocity and the linewidth gives the pressure altitude.

A system using a tunable diode laser has been set-up and characterized. Attempts to measure back-scattered fluorescence were unsuccessful, but inelastic scattering in the forward direction was observed. Mechanisms for this are discussed but no firm conclusion is reached. A correlation technique for processing the data is discussed and its accuracy computed.

TABLE OF CONTENTS

LIST OF FIGURES

LIST OF TABLES

1. INTRODUCTION

The current technique for measuring the speed of supersonic and hypersonic aircraft is a modification of the pitot static tube. One port senses the total impact pressure of the air and another senses the ambient static pressure. The ratio of these two pressures is then used to measure the Mach number. Another sensor measures the impact temperature and with this data the true airspeed can be computed. The main difficulty with this system lies with the measurement of the static pressure. This pressure is very much less than the impact pressure and if the static pressure port sees any part of the impact pressure, then substantial errors occur. Changes in the apparent static pressure do, in fact, occur due to the angle of attack and sideslip of the aircraft. In addition, the port is behind the bow shock of the aircraft and the apparent strength of the shock varies as the aircraft maneuvers.

What is desired is an airspeed sensor which measures the speed of the air ahead of the shock. This air is completely unaffected by the aircraft at supersonic speeds. However, no metalic probe may be placed ahead of the aircraft nose, or it will interfer with radar equipment on the aircraft. A sensor is required which can remotely measure the speed of the air ahead of the aircraft.

A novel type of sensor is suggested which is capable of measuring an aircraft's speed and altitude. The sensor measures the Doppler shift and line width of infra-red radiation resonantly scattered from carbon dioxide molecules in the air. The Doppler shift gives the aircraft speed and the linewidth gives the pressure altitude of the aircraft. Multiple sensors enable the angle of attack and sideslip to be measured. Recently, tunable

semiconductor lasers have become available with very low power consumption and they can be tuned to a very strong resonance of CO_2 at a wavelength of approximately 4.3 μ. The sensor is capable of measuring the air velocity a few feet ahead of the aircraft at altitudes of at least 100,000 ft.

1.1 Previous Laser Doppler Velocimeter Tests

In 1972, Munoz, Mocker and Koehler [5] of NASA Ames and Honeywell flew a carbon dioxide laser-powered Laser Doppler Velocimeter on a NASA CV 990 aircraft. This system used a 25-50 watt laser which required a large power supply and a heat exchanger for cooling. The system worked well up to an altitude of 10,000 ft and an air-speed of 500 kts. The system operated on the principle of measuring the Doppler shift of infra-red radiation at a 10.6 micron wavelength being scattered from naturally occurring aerosol particles in the air. However, at an altitude of greater than 10,000 ft, there was an insufficient number of aerosol particles in the air to give an adequate signal strength. Accordingly, at higher speeds and higher atltitudes, a stronger scattering source than natural aerosols is required.

1.2 Scattering From the Air

The scattering of light traveling through the air can be due to one of four mechanisms:

1. Aerosol scattering.
2. Rayleigh scattering (due to density fluctuations).
3. Raman scattering (stimulated fluorescence).
4. Resonant scattering (natural fluorescence).

The first three mechanisms are all extremely weak and only resonant scattering is strong enough to be used for remote velocity measurement.

Nitrogen and oxygen have strong resonant lines in the ultraviolet, but no radiating ones in the infra-red where tunable lasers operate. Only tri-atomic molecules have radiating resonant lines in the infra-red. The three most common tri-atomic molecules are carbon dioxide, water vapor and ozone. The ozone lines are fairly weak and water is not nearly as common as carbon dioxide in the stratosphere (see Fig. 1) [1]. Thus, CO_2 is the best candidate for a scattering material and this has some strong resonance lines at a wavelength of 4.3 μ.

The CO_2 molecules are excited from their ground state to the 00°1 state when they absorb radiation at 4.3 μ. This is an extremely favorable transition with a cross section of approximately 10^{-16} cm^2 per molecule. Thus, from Fig. 1, at 100,000 ft, radiation at 4.3 μ is attenuated at a rate of 1 per meter. This line is the pumping level in the CO_2 laser. The excited molecules can decay in a number of ways:

1. Transition-to-ground state – radiation at 4.3 μ.
2. Collision with another molecule – energy transferred into translational form.
3. Transition to a lower state (10°0 or 02°0) – radiation at 10.6 μ or 9.5 μ.

It is this reradiation of the original 4.3 μ energy which we propose to use for the measurement of the aircraft speed. Kildal and Byer (1971) [3] have examined this process of resonant backscatter in their review paper and have considered it to be practical for the detection of pollutants, providing the appropriate laser wavelengths can be found.

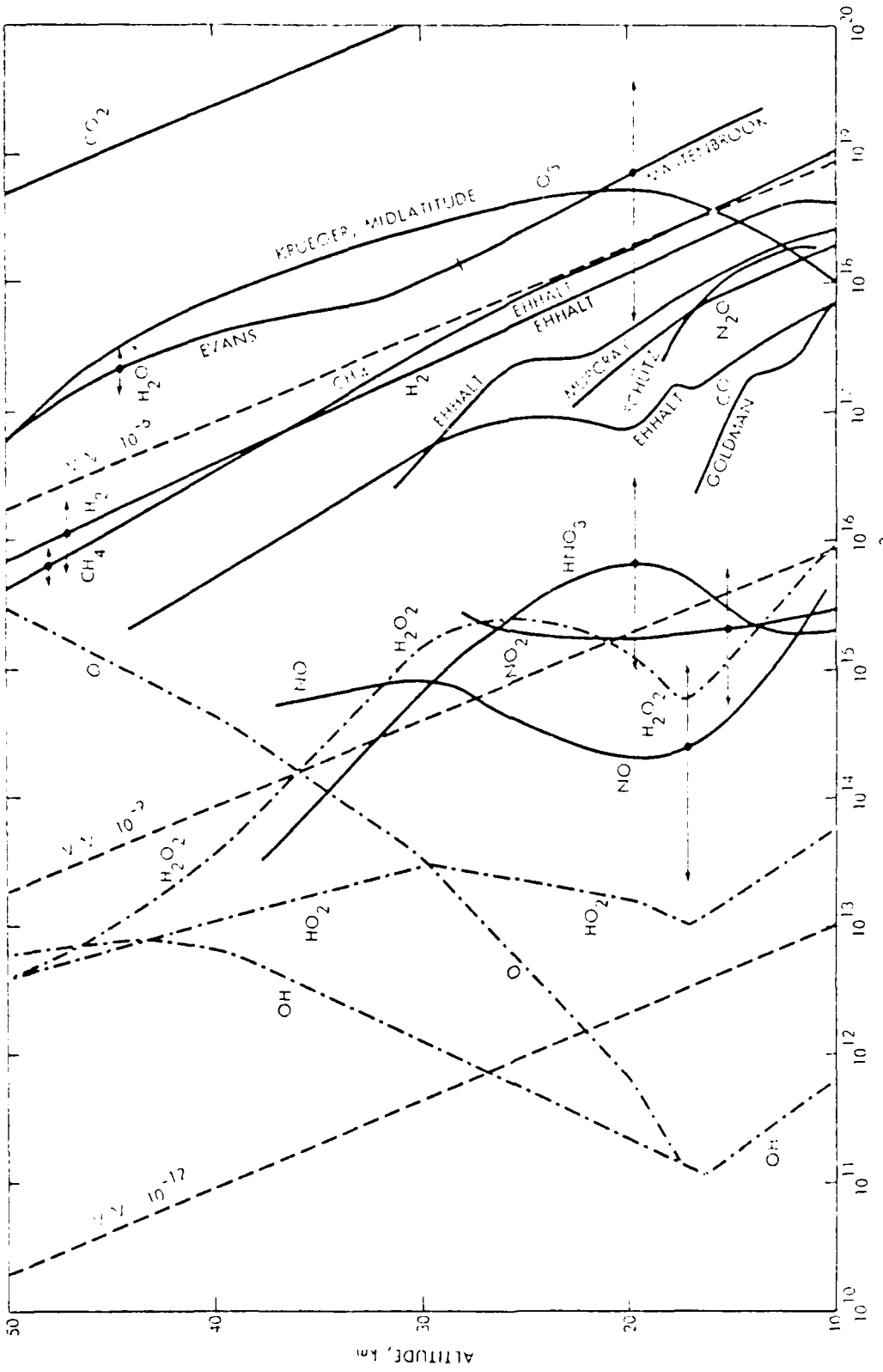

FIG. 1. MINOR SPECIES CONCENTRATIONS IN THE STRATOSPHERE.

The scattering efficiency of the molecule (g) is determined by the ratio of the transition probability for radiative decay, k_r, and the probability for nonradiative decay through collisions, k_c. k_r is a function only of the molecule and is independent of temperature and pressure; it has a value of approximately $k_r = 30$ sec^{-1} (Kildal and Byer, 1971) [3]. k_c, on the other hand, depends on the molecule and other gases present as well as the temperature and pressure. Cheo (1968) [2] has measured the fluorescent decay in a CO_2 laser at low pressures and obtained values of 400 sec^{-1} for pure CO_2 at 1 torr pressure. This was halved however, by the addition of 8 torr of nitrogen. Nitrogen has an excited level very close to that of CO_2 and, hence, helps stabilize it. Sequin and Carswell (1972) [6] have measured the fluorescence up to 760 torr (sea level pressure) and have found the pressure and constituent dependence to be very complex. However, the nonradiative transition probability does increase with pressure and temperature. We might expect a value of 100,000 sec^{-1} at sea level and 2000 sec^{-01} at an altitude of 100,000 ft. The scattering efficiency g is given by

$$\frac{k_r}{k_c} = g \approx \begin{cases} .1\% \text{ at sea level} \\ 15\% \text{ at } 100{,}000 \text{ ft} . \end{cases} \qquad (1)$$

1.3 The Laser Source

Over recent years, there has been much work on the development of tunable infra-red lasers (Melngailis and Mooradian, 1975) [4]. These lasers are made of lead salts such as lead tin telluride, lead gallium telluride, lead sulphide selenide and lead sulphide. They can operate over a wavelength range of 3 - 30 μ depending on the chemical composition. Fine tuning is achieved by changing the temperature of the laser. The laser

has a linewidth of about 3 MHz and is capable of resolving extremely fine spectroscopic detail. These lasers are exceedingly small and operate continuously at a current of a few hundred milliamps. They do, however, require cooling to 10 - 100°K.

The lead salt laser diode system was procured from Laser Analytics Inc. of Lexington, Massachusetts. This company supplied a complete lead salt laser diode system. This consisted of the refrigerator, cryostat, temperature controller, and laser controller.

1.4 Resonance Linewidth

The laser itself has a very narrow spectral width of 3 MHz. The width of the resonance line of CO_2 is much larger and determined by two factors:

1. Doppler broadening, and
2. Pressure broadening.

The former is caused by the Doppler shift from the thermal motion of the CO_2 molecules. The broadening is 198 MHz for CO_2 at a temperature of -55°C. The pressure broadening is due to collisions with other molecules. Its magnitude is about 4 MHz per millibar of atmospheric pressure. Thus, at a pressure of 100 millibars we have a linewidth of about 400 MHz and at sea level will have a linewidth of 4 GHz. It is this pressure broadening which primarily determines the width of the resonance line. Measurement of this linewidth will enable the altitude of an aircraft to be measured.

1.5 Signal Detection

The scattered fluorescence can be detected in one of two ways; either directly or by heterodyne detection. The direct dection is the most straightforward, but the heterodyne detection promises greater sensitivity. In heterodyne detection the scattered radiation is caused to beat with the original laser output to give noise free amplification. Heterodyne detection does, however, have inefficiencies not present in direct detection schemes. Beam splitter/combiner losses are 30%. Radiation is scattered into other rotation lines and not detected (90% lost) and the bandwidth of the detector is less than that of the line of CO_2 (90% lost). This gives an overall efficiency of only 0.2% at most. However, heterodyne detection does have the potential for one to two orders of magnitude greater sensitivity than direct detection. An Indium Antimonide detector has been used.

1.6 Operation of the Sensor

The laser is tuned to a 4.3 u resonant line of the CO_2. The frequency of the laser is then scanned by a ramp waveform, on the current, which will drive the laser through the resonance line. The output of the reference detector can be monitored directly since the signal is strong and of small bandwidth. This detector shows a peak in the absorption of the laser radiation by the reference cell of CO_2, corresponding to zero velocity. The width of the absorption peak corresponds to the known pressure of the CO_2 in the reference cell.

The output of the heterodyne detector is treated a little differently. It is first amplified by a wide band preamplifier of bandwidth ΔF and then detected, or squared, and integrated with a bandwidth Δf. This enhances the signal-to-noise ratio by

a factor of $\Delta F/\Delta f$ over the raw signal. The heterodyne detector output is then correlated with the reference detector output. The frequency shift between the peaks is

$$.238V \text{ MHz} \tag{2}$$

where V is the aircraft speed in kts, and the atmospheric pressure is obtained from the width of the heterodyne detector peak and is

$$(16\ p^2 + \Delta d^2)^{\frac{1}{2}} \text{ MHz} \tag{3}$$

where p is the pressure in millibars and Δd is the linewidth due to the motion of the carbon dioxide molecules. At a temperature of -55°C, this linewidth is 188 MHz. It would appear that the accuracy of this technique of altitude measurement would be poor above 30,000 ft because the linewidth is determined more by the Doppler broadening than by the pressure broadening above that altitude.

The lowest airspeed which can be measured with this sytem depends upon how small a fractional shift in the line we can measure. A speed of 100 kts corresponds to a shift of 23.8 MHz. At sea level, this represents approximately 1/2% of the linewidth; at 30,000 ft it is 1½% and at 100,000 ft is it 12%. Thus, low speeds are easier to measure at high altitude.

2. CALCULATION OF SIGNAL STRENGTH

2.1 Introduction

This section discusses the signal strength to be expected for the detection of fluorescence from carbon dioxide. First, we will consider the strength obtained by heterodyne detection of the backscattered fluorescent radiation. Then we will compare this with the signal obtained by forward scattering. Finally, we will consider which type of photodetector is most suitable for use in the heterodyne detection of radiation.

2.2 Signal for Backscattered Heterodyne Detection

The most sensitive method for detecting the backscattered signal from the carbon dioxide is by heterodyne detection. Here the signal radiation is mixed with original laser radiation and the two beat together. Because a photodetector is a square law device, the resulting photocurrent is proportional to the square root of the product of the laser and the signal intensities. This results in a noise free boost in the signal level.

In heterodyne detection, the detector noise itself is not relevant since the local oscillator can always be made strong enough so that the detector is shot noise limited in the signal. The photocurrent of the signal, I_s, is given by

$$I_s = 2\sqrt{P_s P_{LO}}\, R \qquad (4)$$

where P_s = signal power

P_{LO} = local oscillator power

R = responsivity of the detector (amps/watts).

The noise in the detector arises from shot noise due to the

photocurrent from the local oscillator. This noise, I_N, must be larger than the intrinsic noise i_n. Then

$$I_n^2 = 2eP_{LO}R\Delta f \qquad (5)$$

where e = charge on the electron = 1.6×10^{-19} Coulombs and

Δf = bandwidth of the system.

Therefore,

$$\frac{I_S^2}{I_n^2} = \frac{2P_S R}{e\Delta f} \qquad (6)$$

which is only a function of the signal power and not the local oscillator power.

Let us now square the photodetector output and define

$$\frac{S+N}{N} = \frac{(I_N+I_S)^2}{I_N^2}$$

$$= 1 + 2\frac{I_S}{I_N} + \frac{I_S^2}{I_N^2} \qquad (7)$$

If $I_S << I_N$ we can drop the last term. Then,

$$\left(\frac{S}{N}\right)^2 = 2\frac{I_S^2}{I_N^2} = \frac{4P_S R}{e\Delta f} \quad . \qquad (8)$$

Now if we integrate the output of square, Δf becomes the bandwidth of the integrator. Therefore, the output signal to noise

power ratio is

$$\left(\frac{S}{N}\right)^2 = \frac{4P_s R}{e\Delta f} \quad . \tag{9}$$

Let us now consider the signal power P_s backscattered from the carbon dioxide. Let the receiver lens have a radius r and let the focal volume be at a distance R from the lens (Fig. 2). Then

$$P_s = P_0 \frac{\pi r^2}{4\pi R^2} \eta k \Delta L \, (\exp -2kL) \tag{10}$$

where P_0 = initial laser power

η = fraction of absorbed radiation remitted

k = absorption coefficient

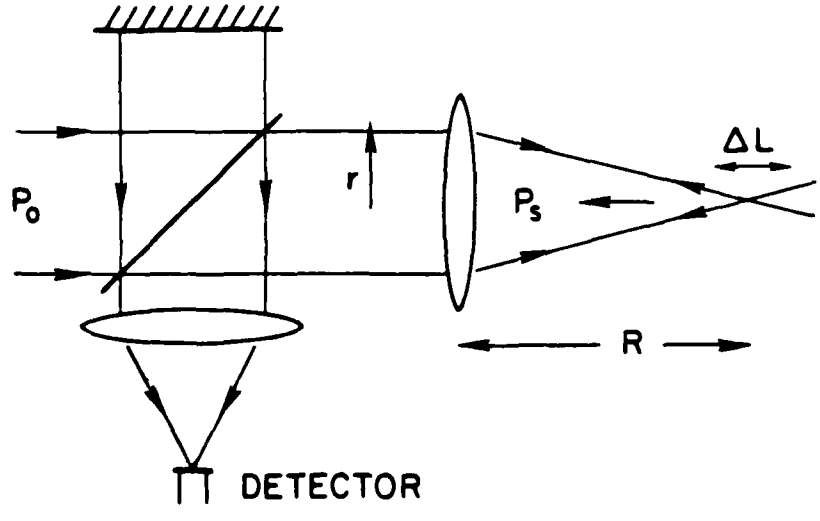

FIG. 2. GEOMETRY OF BACKSCATTERING.

ΔL = coherent depth of field = $\frac{\lambda R^2}{2r^2}$

λ = wavelength of laser.

Then,

$$P_s = P_0 \frac{\lambda}{8} \pi k \, (\exp -2kL) \, . \qquad (11)$$

This is independent of the receiver.

Now this power is distributed over the whole natural linewidth Δn, whereas we can only detect that part within the detector bandwidth ΔF. This reduces the effective power by $\Delta F/\Delta n$. Hence, signal-to-noise ratio is

$$\left(\frac{S}{N}\right)^2 = \frac{P_0 R \Delta F \pi \lambda k}{2e\Delta f \Delta n} \, (\exp -2kL) \, . \qquad (12)$$

For P_0 = 100 μwatts,

R = 2 amps/watt,

$\Delta F/\Delta n$ = .01,

Δf = 100 Hz,

g = 0.001,

$\lambda = 5 \times 10^{-6}$ m,

$k = 1 \, m^{-1}$

L = 1 m, then

$\left(\frac{S}{N}\right)^2$ = 30 or 15 dB .

Alternatively if we are detecting spontaneously emitted radiation from a black body, then from Plancks radiation law

$$P_s = \frac{2hn\Delta F}{\lambda^2[\exp(hn/kT)-1]} \text{ watts/meter/steradian} \quad (13)$$

where h = Planck's constant = 6.625×10^{-34} watts sec

k = Boltzman's constant = 1.38×10^{-23} watt sec/deg°K

n,λ = frequency and wavelength of radiation = 7×10^{13} Hz, 4.27 μm

T = temperature of body = 300°K.

Then, $P_s = 6.44 \times 10^{-14}$ ΔF watts/meter^2/steradians.

For heterodyne detection, the product of area and spherical field of view is determined by coherence. For a laser in a TEM_{oo} mode, this product can be shown to be $0.918\lambda^2$. For other modes the numberical factor differs slightly. Then

$$P_s = 1.06 \times 10^{-24} \Delta F \text{ watts} \quad (14)$$

and

$$\left(\frac{S}{N}\right)^2 = 3.2 \times 10^{-5} \frac{R\Delta F}{\Delta f} \quad . \quad (15)$$

For both of these heterodyne schemes we require a detection with a large responsivity-bandwidth product and an integrator with a long time constant.

2.3 Calculation of Forward Heterodyne Signal

Let us consider a convergent laser beam (half angle α) falling on a photodetector of radius a and covering it (Fig. 3). The laser radiation is scattered by a CO_2 molecule and some of this radiation also falls on the photodetector. Here the scattered and direct radiation beat together to give a heterodyne signal.

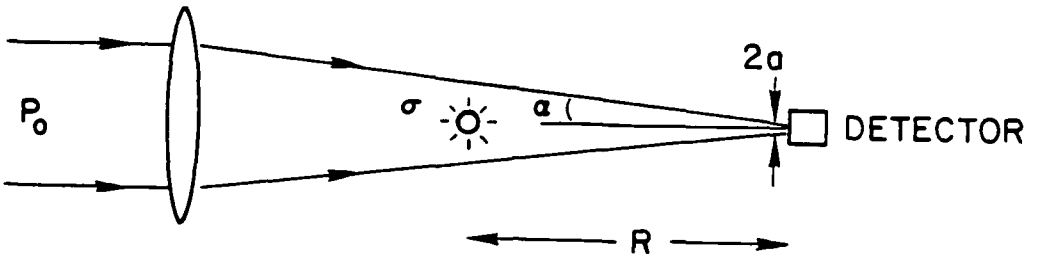

FIG. 3. GEOMETRY OF FORWARD SCATTERING.

The direct beam power = $P_0 \exp(-kL)$, where P_0 = initial laser power, k = attenuation coefficient, and L = path length through the air. The scattered beam power = $P_0 \exp[-k(L)] \pi a^2/4\pi R^2 \times \sigma/\pi(\alpha R+a)^2$, supposing the scattering is isotropic and that the scattering center is at a distance R from the photodetector and σ is the scattering cross-section.

Now, if the scattered and the direct wavefronts have parallel wavefronts, there will be perfect mixing and the heterodyne signal will be the square root of the product which is

$$P_0 \exp(-kL) \frac{a}{2R(\alpha R+a)} \left(\frac{\sigma}{\pi} \frac{\Delta F}{\Delta n}\right)^{1/2}$$

where Δn = molecular linewidth and ΔF = photodetector bandwidth. Now we can write the scattering cross section σ as

$$\sigma = k_s/N \ ,$$

where g = that fraction of the absorbed energy which is scattered and N = number of molecules per unit volume.

We will now integrate over the volume of the beam to obtain the total scattered beam power on the photodetector which is

$$\int P_0 \exp(-kL) \frac{\pi a^2}{4\pi R^2} \frac{k_s}{\pi(\alpha R+a)^2} dV$$

$$= \frac{P_0 k g a^2}{4} \exp(-kL) \int \frac{1}{R^2} dR$$

$$= \frac{P_0 k g a^2}{4} \exp(-kL)/R_{min} \ .$$

R_{min} is the detector window distance which is 1.27 cm in our case.

If the scattered waves have the same wavefront as the direct wave, then the heterodyne current from Δ is

$$P_0 R_a \exp(-kL) \left(\frac{kg\Delta f}{R_{min}\Delta\nu}\right)^{\frac{1}{2}} \ .$$

In practice the scattered and direct wavefronts are not coincident.

The phase difference at a distance r off-axis is

$$\phi = \frac{2\pi}{\lambda} \frac{r^2}{2} \left(\frac{\alpha}{a} + \frac{1}{R}\right) \ .$$

The average phase of the signal is

$$\Phi = \frac{1}{\pi a^2} \int_0^a 2\pi r \phi dr$$

$$= \frac{\pi a}{4\lambda} \left(\alpha + \frac{a}{R}\right) .$$

The average phase of the whole scattered beam is

$$\Phi = R_{min} \frac{\pi a}{4\lambda} \int_{R_{min}}^{\infty} \frac{1}{R^2} \left(\alpha + \frac{a}{R}\right) dR$$

$$= R_{min} \frac{\pi a}{4\lambda} \left(\frac{\alpha}{R_{min}} + \frac{a}{2R_{min}^2}\right)$$

$$= \Phi(2R_{min})$$

or the mean phase is that scattered from a distance of twice R_{min}. The heterodyne current is proportional to cosine Φ and is equal to

$$P_0 Ra \exp(-kL) \left(\frac{kg\Delta F}{R_{min}\Delta\nu}\right)^{\frac{1}{2}} \cos\left(\frac{\pi a}{4\lambda} (\alpha + a/2R_{min})\right) .$$

The depth of modulation is then divided by P_0. Now, if we take $a = 0.25$ mm, $k = .010$ mm, $L = .2$ m, $g = 10^{-2}$, $\Delta f/\Delta\nu = 10^{-2}$, $R_{min} = 12.5$ mm, and $\alpha = .012$ rads, depth of modulation = 2.5×10^{-6}.

2.4 Ratio of Forward to Backscattered Signal Currents

This ratio is

$$a\left(\frac{\delta}{R_{min}\lambda}\right)^{\frac{1}{2}} \cos\left[\frac{\pi a}{4\lambda} \left(\alpha + \frac{a}{2R_{min}}\right)\right] \exp(kL)$$

which is of the order unity for weak lines. Thus, the forward and backscattered are comparable as long as the absorption is not too strong.

2.5 Selection of Photodetector

2.5.1 Introduction

The selection of a photodetector for the Laser Doppler Airspeed Sensor must be made carefully if we are to achieve optimum performance for the system. However, the figure of merit used to compare detectors is different for whether direct detection or heterodyne detection is employed. These figures of merit will be derived and, as may be expected, a different detector is optimum in the two cases. There are three basic types of detector:

1. Thermal (pyro-electric or thermopile)
2. Photo-conductive (current α light level)
3. Photo-voltaic (voltage α light level).

These various materials are detailed in Table 1. Thermal detectors are quickly dismissed as being much less sensitive than the other types. Photo-voltaic detectors are, in fact, the most promising since they are much faster than photo-conductive types. The two materials with good sensitivity at the wavelength of interest (4.3 micrometers) are Indium Antimonide and Mercury Cadmium Telluride. Of these, the former is an inherently quieter detector.

2.5.2 Detectivity

For conventional, direct detection the figure of merit for a detector is called its detectivity or D*. This is the reciprocal

of the equivalent detectable power of the noise of the detector of unit area and unit bandwidth. It is generally expressed as 1/[Watts per centimeter per (Hertz)$^{1/2}$]. The higher the D*, the smaller the amount of power which can be detected.

TABLE 1. COMPARISON OF PHOTODETECTOR MATERIALS.

Material	Type	Temperature	Responsivity (R)	Detectivity	Response Time (τ)	R/τ
$LiTaO_3$	Pyroelectric	298°K	1.5×10^{-6} amp/watt	1×10^{8}	150 n sec	10
PbSe	Photoconductive	240°K	1.3×10^{-2} amp/watt	1.3×10^{10}	25 μ sec	500
InSb	Photovoltaic	77°K	2 amp/watt	1×10^{11}	20 n sec	10^{9}
Ge:Au	Photoconductive	77°K	1×10^{-2} amp/watt	3×10^{9}	2 n sec	5×10^{6}
(HgCd)Te	Photoconductive	77°K	4 amp/watt	10^{10}	250 n sec	4×10^{7}
(HgCd)Te	Photovoltaic	77°K	1.2 amp/watt	2×10^{9}	3 n sec	4×10^{8}
(PbSn)Te	Photovoltaic	77°K	2.5 amp/watt	2×10^{10}	1 μ sec	2.5×10^{6}

The detectivity of a device may be determined either by its own internal noise or by noise in the ambient background (Background Limited Performance, BLIP). At room temperature all detectors are limited by their intrinsic noise. However if they are cooled, this decreases until they become background limited. Therefore, most detectors are cooled by liquid nitrogen in order to obtain BLIP, even though they will operate at room temperature.

The BLIP can still vary between detectors since it can vary with the amount of background that the detector sees. It is a function of:

1. Spectral reponse of detector.
2. Temperature of the background.
3. Field of view of detector.

Shorter wavelength detectors will have a higher D* because they are less sensitive to the background. Generally the optimum detector has the following features:

1. Detector not sensitive to wavelengths longer than those of interest.
2. A Cold Filter can be placed over the detector to limit its spectral response.
3. A Cold Shield limits the field of view of the detector.
4. Detector is made as small as practical.

Using all these features, it is practical to get down to a noise level equivalent to 10^{-16} watts of signal in a 1 Hz bandwidth.

2.5.3 Heterodyne detection

In Sec. 2.2, the discussion on heterodyne detection, it was shown that the important parameter in evaluating the performance of the photodetector was the product of the responsivity and the bandwidth of the detector. Therefore, we shall define

Figure of merit = responsivity × bandwidth of detector.

2.5.4 Local oscillator power

In heterodyne detection, the process is shot noise limited, providing that the local oscillator is strong enough that its own shot noise dominates all other noise in the photodetector. These sources are:

1. Background or detector noise as described by the detectivity of the detector.
2. Preamplifier noise.
3. Laser noise.

The relative performance of Indium Antimonide and Mercury Cadmium Telluride are given in Table 2.

TABLE 2. TWO HETERODYNE PHOTODETECTORS.

	Indium Antimonide (SBRC)	Mercury Cadmium Telluride (Honeywell DLK146)
Detectivity (watts cm Hz)$^{\frac{1}{2}}$	3×10^{11}	2×10^{9}
Diameter (mm)	0.5	0.375
Bandwidth (MHz)	20	100
Photodetector NEP (watts)	7×10^{-10}	1.8×10^{-7}
Amplifier NEP (watts)	2.2×10^{-8}	1×10^{-8}
Responsivity (amps/watts)	2.0	1.2
Local Oscillator Power Minimum (milliwatts)	0.15	1.4
Responsivity × Bandwidth (amps MHz/watts)	40	120

The distinction between detector noise and preamplifier noise is sometimes a little difficult to make. At the wide bandwidths used for heterodyne detection, no detector is background noise limited, but rather limited by thermal or Johnson noise generated by the impedance of the photodetector as seen by the preamplifier. The lower this impedance the greater the noise equivalent power. The performance of Indium Antimonide is determined by its junction capacitance which is about 100 pf for a 1/2 mm detector. In the case of Mercury Cadmium Telluride, the junction capacitance is about the same, but the dynamic impedance is very low, about 30 ohms, which makes the detector appear very noisy. The penultimate line in Table 2 details the local oscillator power required for shot noise limited heterodyne detection.

This power is 1.4 millwatts for Mercury Cadmium Telluride, but only 0.15 millwatts for Indium Antimonide. Under this program it is not expected that more than a few hundred microwatts of local oscillator power will be available from the diode laser and therefore shot noise operation could not be obtained from the Mercury Cadmium Telluride detector.

Finally, laser noise may prevent shot noise limited operation of the heterodyne detector. This noise increases directly with laser power and cannot be overcome.

2.5.5 Choice of photodetector

For direct detection of infrared radiation with a wavelength of 4.27 micrometers at frequencies below 1 MHz, photovoltaic Indium Antimonide or photoconductive Mercury Cadmium Telluride detectors are the most suitable. For heterodyne detection, photovoltaic Mercury Cadmium Telluride detectors have the best figure of merit, but the ocal oscillator power required is more than we have available. Therefore an Indium Antimonide detector was used in both cases. One was procured from the Santa Barbara Research Center, along with two matched preamplifiers — one for low frequency direct detection and one for high frequency heterodyne detection.

The data described here are based upon commercially available detectors and does not necessarily represent the ultimate state of the art.

3. CHARACTERIZATION OF CARBON DIOXIDE LINES

Carbon dioxide has three modes of vibration. Since it is a linear molecule there are (Fig. 4)

a. Symmetric mode (100) — The carbon atom is stationary and the oxygens move in opposite directions in the line of the molecule.

b. Bending mode (degenerate 010) — The oxygens move together, perpendicular to the line of the molecule.

c. Asymmetric mode (001) — One oxygen and the carbon move one way and the other oxygen moves in the opposite direction in the line of the molecule.

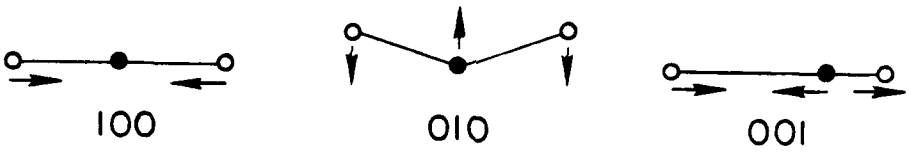

FIG. 4. CO_2 VIBRATION MODES.

Since the first two modes are symmetric, they cannot have any net electric dipole moment. Thus, only the 001 mode can be excited by an electromagnetic field. It is this mode that we are employing in this study. This mode has a natural frequency corresponding to a wavelength of 4256.7 nm (in vaccuo).

The spectrum is complicated, however, by the fact that the CO_2 molecules are also rotating and, since a photon contains angular momentum, the CO_2 molecule must also change its angular momentum when it emits or absorbs radiation.

The rotational kinetic energy, E_J of the molecule is

$$\frac{E_J}{hc} = BJ(J+1) - DJ^2(J+1)^2$$

where h = Plancks constant, c = speed of light,

J = rotational quantum number,

$$B = \frac{h}{8\pi^2 c I_B} = \frac{27.994 \times 10^{-40}}{I_B} \text{ cm}^{-1} = 0.3895 \text{ cm}^{-1} \text{ for } CO_2 \text{ in ground state}$$

I_B = moment of inertia of the molecule

D = stretching term due to centrifugal force = $B^3/\pi^2\nu_0^2$

ν_0 = natural resonant frequency of the molecule.

However, in $^{12}C^{16}O_2$, the atomic spins are zero, and symmetry rules then require that odd values of J are forbidden. Therefore, the selection rule for any transition is $\Delta J = 0, \pm 2$. However, if $\Delta J = 0$, the angular momentum of the emitted or absorbed photon is not conserved. Therefore

$$\Delta J = \pm 2 \ .$$

If $\Delta J = -2$, the transition is said to be in the P branch and if $\Delta J = +2$, it is said to be in the R branch. The wavenumbers in the two branches are (Herzberg, 1945)

$$P(J) = \frac{\nu_0}{c} - (B'+B'')J + (B'-B'')J^2$$

$$R(J) = \frac{\nu_0}{c} + 2B' + (3B'-B'')J + (B'-B'')J^2$$

where $B' = 0.3866 \text{ cm}^{-1}$ and $B'' = 0.3895 \text{ cm}^{-1}$ are the rotational

constants of the 001 and 000 levels, respectively, and J is the rotational quantum number of the lower state. These may be summarized as

$$\frac{\nu}{c} = 2349.2 + .7761\ m - .0029\ m^2\ cm^{-1}$$

where m = -J for the P branch and m = J+1 for the R branch.

The intensity of each line is determined by the population of the initial state. This, in turn, is determined by the thermal Boltzman distribution. The P and R branches are symmetrical. This gives rise to the familiar "butterfly" which is illustrated in Fig. 5.

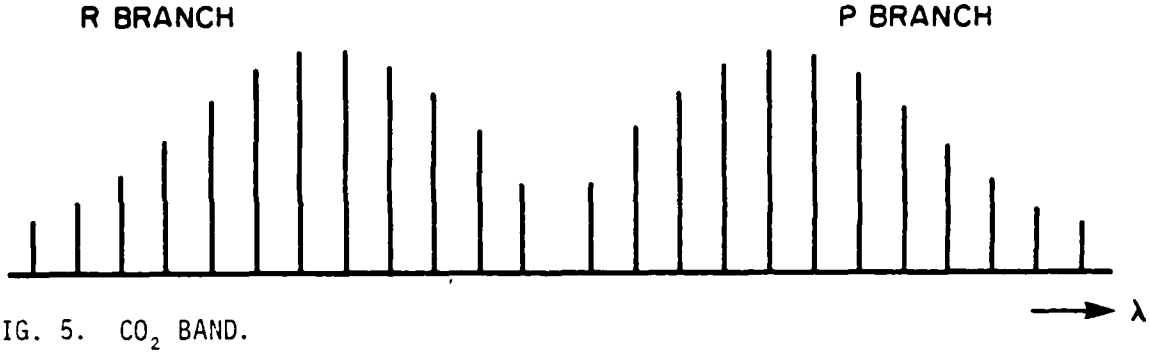

FIG. 5. CO_2 BAND.

The population of the J level N(J) is given by

$$N(J) \propto (2J+1)\ \exp(-E_J/kT) \text{ for J even only}$$

$$\propto (2J+1)\ \exp[\{-J(J+1) + .0037J^2(J+1)^2\}/535.3]$$

at 300°K.

This has a maximum for a J value of approximately 16 at room temperature (300°K).

The exact frequencies of the P branch of the 4.25 μm branch of CO_2 have been calculated and are given in Table 3.

TABLE 3. WAVELENGTHS OF P BRANCH OF 4.25 BAND OF CO_2.

J	Wavelength (μm) in Vacuum
0	4.2567
2	4.2595
4	4.2624
6	4.2654
8	4.2683
10	4.2714
12	4.2744
14	4.2775
16	4.2807
18	4.2839
20	4.2872
22	4.2905
24	4.2938
26	4.2972
28	4.3007
30	4.3042
32	4.3077
34	4.3113
36	4.3149
38	4.3186
40	4.3224

The laser diode has been used to identify as many of the CO_2 lines as possible and measure their strength. The results are shown in Fig. 4. Laser No. 1 was tuned over the range from

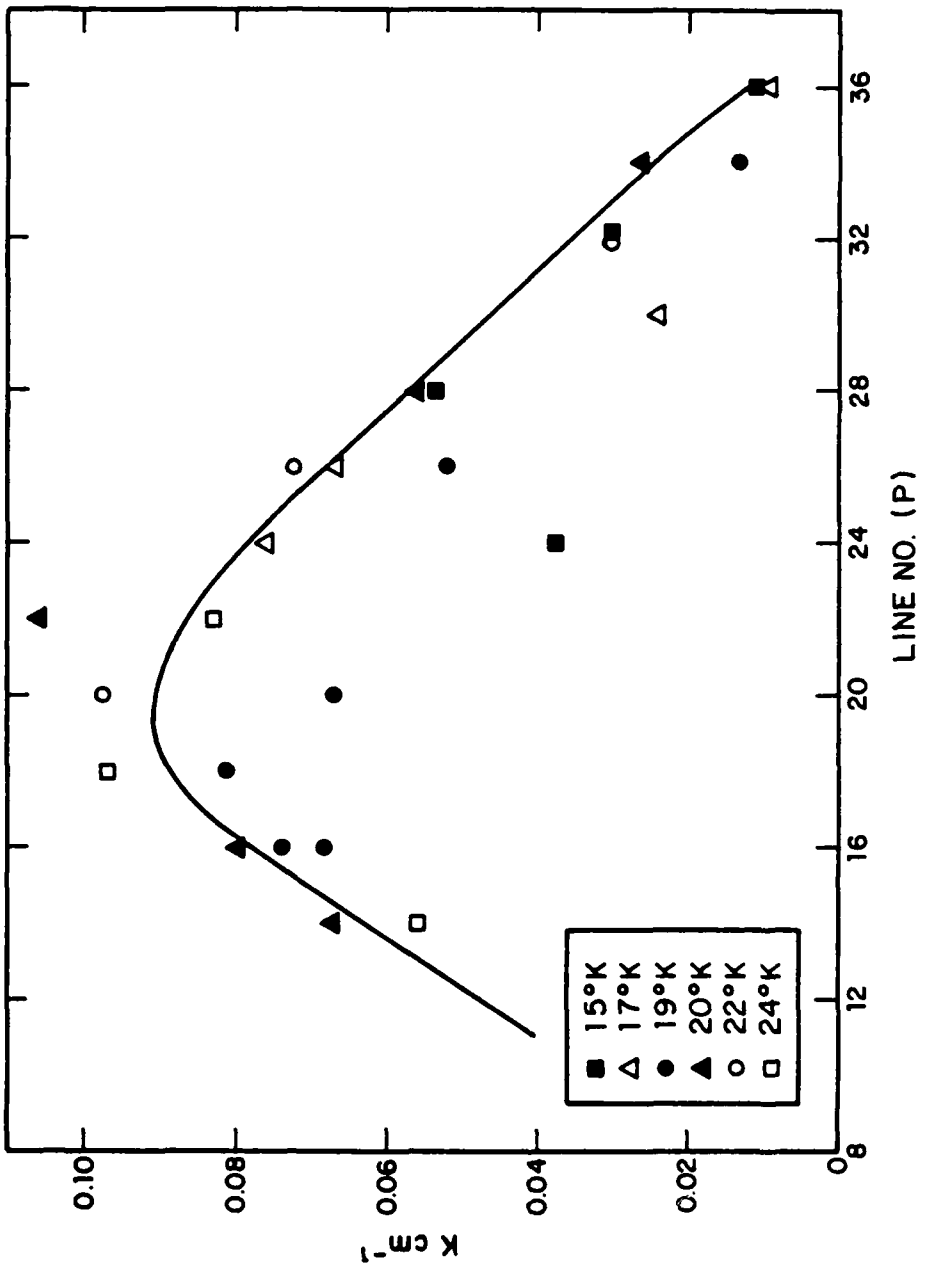

FIG. 6. CO_2 LINE STRENGTHS IN AMBIENT AIR.

P(14) to P(36). The peak appears to occur at P(20) whereas we would have expected a peak at P(16). However, since we could not identify the center of the band, we have had to rely on the absolute wavelength to identify the J number. This has an error of ±2 nm or ±2 in the J number. Thus, we could be in error by 2 in the J numbers assigned to the lines.

4. EXPERIMENTAL MEASUREMENTS

The main purpose of this program is to measure the resonant fluorescence of carbon dioxide in the 4.25 μm band. This can be done by one of three techniques:

1. Direct detection.
2. Heterodyne detection.
3. Heterodyne detection of the background.

The experimental arrangements for these three techniques are shown in Figs. 7 - 9. An Indium Antimonide detector (cooled by liquid nitrogen) was used for the reasons given in Sec. 2.

The Laser Analytics Laser Cold Head was mounted on a Newport Research Corporation Optical Breadboard, 2 ft x 4 ft. The head was mounted on posts so that the laser diode was 6 in. above the table. The whole optical system was then kept at this height. This greatly eased the alignment. The laser output beam was quite narrow (100 mrad divergence) but at an odd angle to the optical axis. Accordingly, the output is collected by a 1-in. diam f/1 lens made of Irtran 2 (zinc sulphide). This is an aspheric lens and is available from Eastman Kodak. This then collects the laser output from wherever it may be. Calcium Fluoride lenses and a beam splitter were used. A lead selenide detector, which is thermoelectrically cooled, is used as a beam monitor and an Indium Antimonide detector, which is cooled by liquid nitrogen, is used to detect the signal. This latter detector has two associated preamplifiers; a high gain one (520 V/μwatt) with a bandwidth of 10 kHz, and a high bandwidth one (20 MHz) with a lower sensitivity (0.78 V/μwatt).

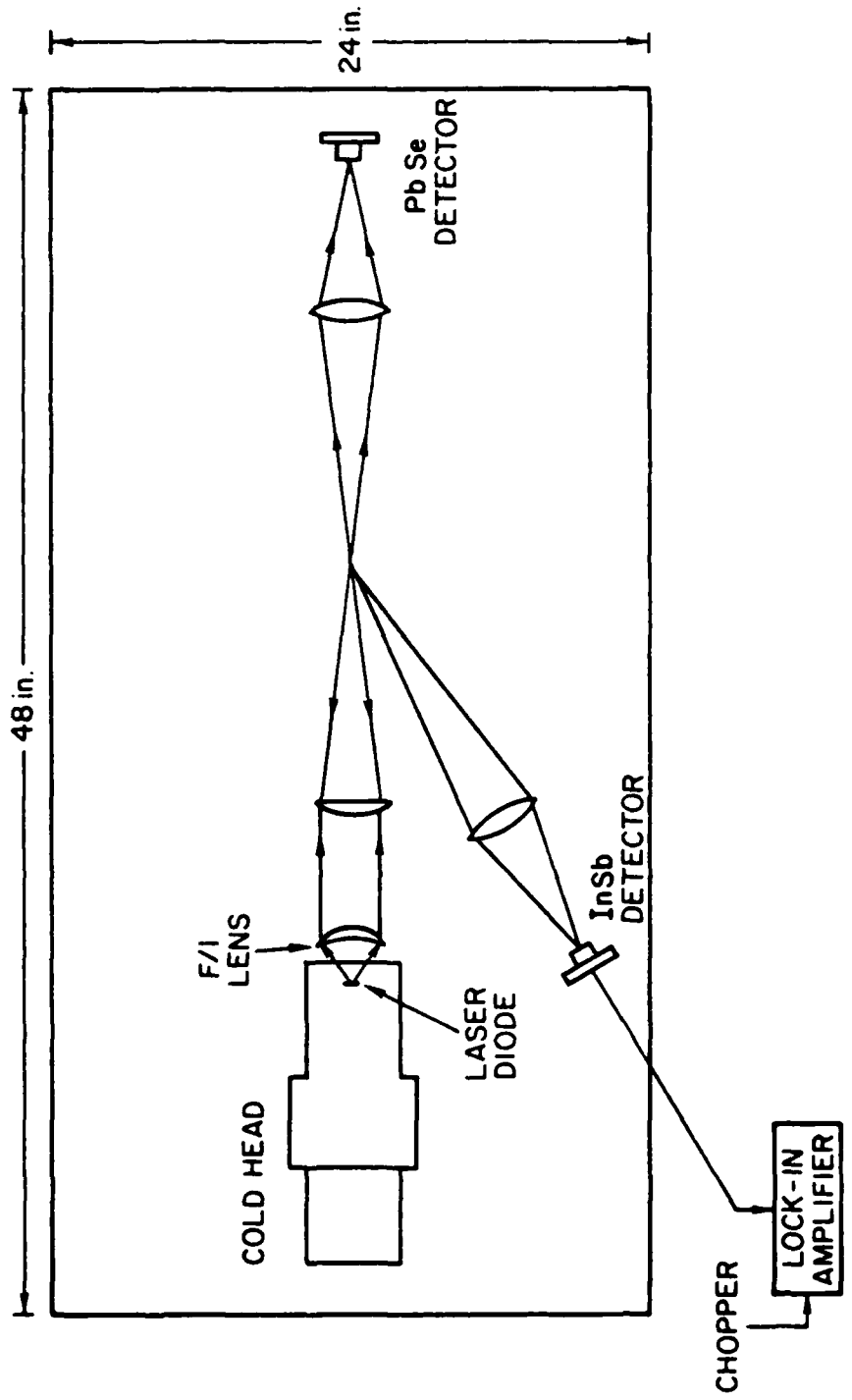

FIG. 7. DIRECT DETECTION.

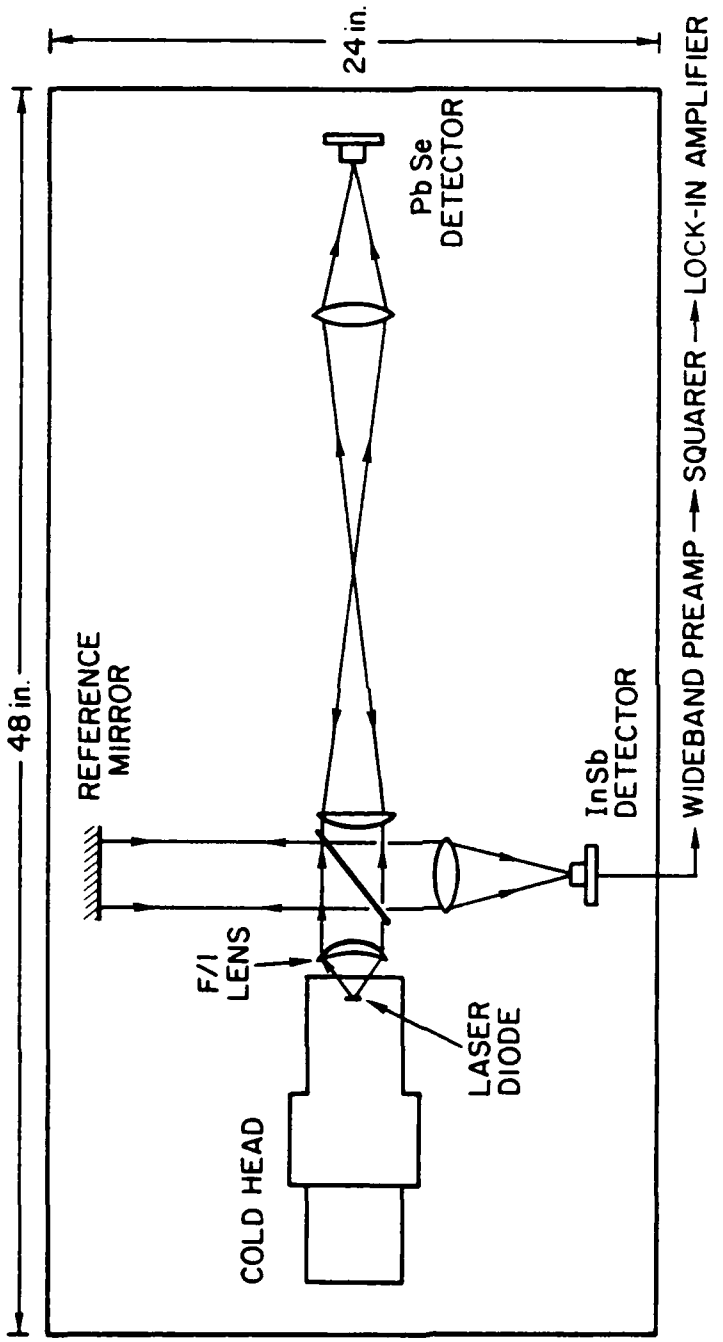

FIG. 8. HETERODYNE DETECTION.

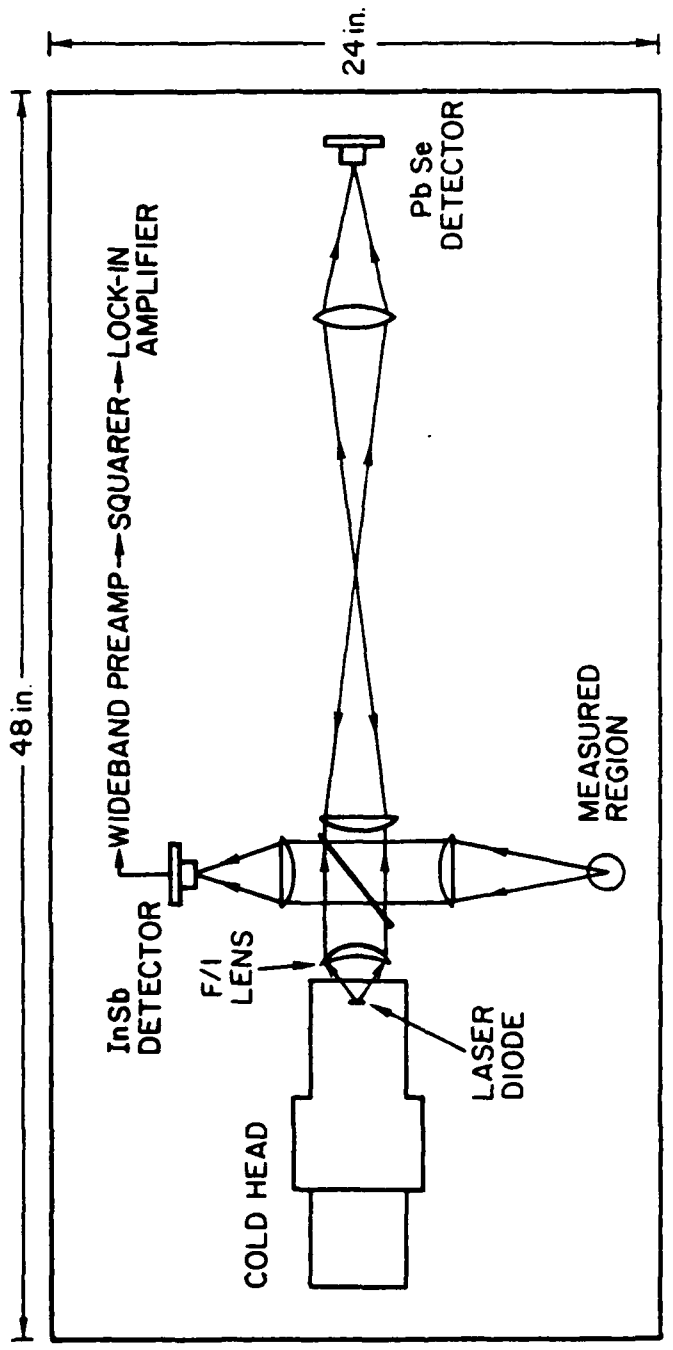

FIG. 9. HETERODYNE DETECTION OF BACKGROUND.

4.1 Direct Detection

The InSb (Indium Antimonide) detector was aligned to look at the same region as the laser was focused. The noise equipment power (NEP) of the detector had been calibrated by the manufacturer as 1.62×10^{-13} watts/$Hz^{\frac{1}{2}}$ or 5.12×10^{-12} watts on a 1 MHz bandwidth. Such low values were achieved because the detector had a cold aperture in front which restricted its field of view to 30°.

The power in the laser beam was measured with the PbSe (Lead Selenide) detector. With the laser in chop mode, a signal of 2.4 Volts was obtained. The manufacturers quoted sensitivity was 24 mV/uwatt at 4.2 μm wavelength. This implies a beam power of 100 uwatt. Now the collecting lens subtended a solid angle of 0.11 steradians and, therefore, collected 1% of the scattered radiation. A depth-of-field of 0.3 mm can be expected for the 0.2 mm detector. For an attenuation coefficient of 0.03 cm^{-1}, 0.1% is scattered in 0.3 mm. Further, as discussed in Sec. 1, at ambient pressure, only 0.1% of the absorbed radiation is re-radiated. Combining all these factors, we obtain an estimated signal strength of 10^{-12} watts.

This signal is one-fifth the estimated noise voltage of 5×10^{-12} watts. Accordingly, it is not surprising that the results of this experiment were negative and no signal could be detected.

4.2 Heterodyne Detection

The experimental arrangement shown in Fig. 7 was set up. The wide bandwidth preamplifier was used. This had a noise equivalent power of 4.22×10^{-12} watt/$Hz^{\frac{1}{2}}$ or 1.33×10^{-8} watts for a 30 MHz bandwidth. This was passed through a 1000 pf

capacitor into a crystal detector (Hewlett Packard 4-TI) with a 50 ohm input impedance. Thus, the detector measured the power in a bandwidth from 3 to 20 MHz. However the low impedance does reduce the sensitivity of the preamplifier to approximately 0.4 V/uwatt. The crystal detector has an effective integration time of 10^{-6} seconds, giving an effective 16 kHz bandwidth. The input power vs output voltage relationship of the detector is shown in Fig. 11. 0 dBm corresponds to 0.28 Volts.

As the laser was scanned, the noise level from the InSb (Indium Antimonide) detector was found to vary in a series of "bursts." At first this was though to be laser mode switching noise. That is, the laser can oscillate in several modes and it switches between them. Indeed, this increase in noise is seen to occur around points of inflexion in the laser power output curve. However many of these noise bursts were found to occur at the same time as a CO_2 absorption line was detected by the Lead Selenide detector. This then was a strange state of affairs, with the detector noise increasing as the incident radiation decreased at an absorption line. Shot noise decrease as the incident radiation decreases. Thus there must be something else producing this noise.

The statistics of the noise were examined on an oscilloscope. The laser mode switch consisted of spikes or square pulses of 10 usecs or so duration. The noise on the CO_2 absorption was quite different. It was "white" with a bandwidth of that of the detector and a Gaussian amplitude distribution. This is just the form we would expect a heterodyne signal to have.

The crucial test that this noise was due to the carbon dioxide was performed by inserting a gas cell between the laser and InSb detector. Then the cell was evacuated. As the pressure

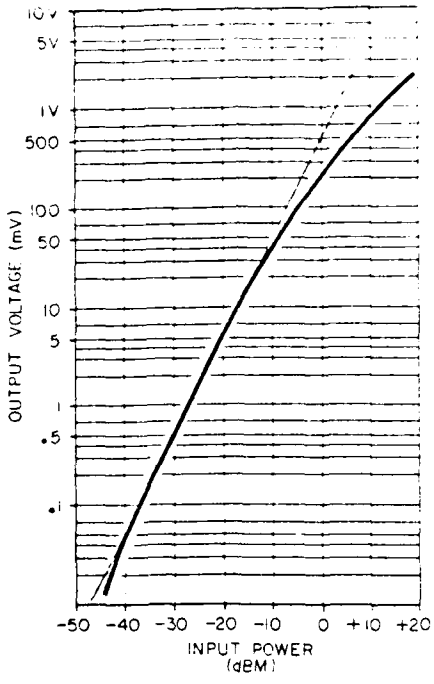

FIG. 10a. 8471A TYPICAL OUTPUT VOLTAGE VS INPUT POWER.

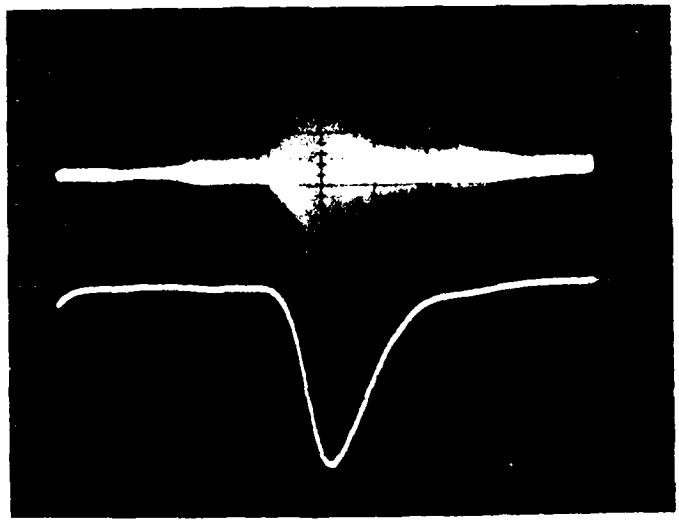

FIG. 10b. PHOTODETECTOR RAW SIGNAL AND DETECTOR OUTPUT (Top 0.2 V/cm, Bottom 0.02 V/cm).

was reduced, the width of the noise burst initially narrowed and then weakened until it disappeared. On reventing to the atmosphere it reappeared. Again, this time at atmospheric pressure, the cell was flushed with helium. Again the noise "burst" disappeared. Conditions in the gas cell could not possibly affect the laser mode switching and, therefore, the noise has to originate from the gas in the cell.

This noise from the CO_2 could be due to one of two processes:

a. Noise inherent in the absorption process.

b. Heterodyne beating of fluorescent radiation.

The noise inherent in the absorption process can consist of the following mechanisms:

1. Photon noise due to fluctuations in the absorption rate.

2. Carbon dioxide density fluctuations.

Photon Noise

The laser beam is made up of discrete photons. Accordingly, there are fluctuations in the arrival rate of the photons and this appears as noise in the output of the photodetector.

$$\text{Arrival rate of photons} = \frac{P_0 e^{-kL}}{h\nu} \text{ per unit time}$$

where h = Plancks constant and ν = frequency of laser light.

$$\text{Noise due to variation in arrival rate} = \left\{\frac{P_0 e^{-kL}}{h\nu}\right\}^{\frac{1}{2}}$$

per unit time.

If the detector has a bandwidth of Δf, the rms noise is

$$\left(\frac{2P_0 e^{-kL}\,\Delta f}{h\nu}\right)^{\frac{1}{2}} .$$

At the same time, the absorption of the photons is a statistical process which generates noise similar to the random arrival rate of photons. This rms noise is

$$\left(\frac{2P_0(1-e^{-kL})\Delta f}{h\nu}\right)^{\frac{1}{2}} .$$

The sum of these two noise mechanisms is

$$\left(\frac{2P_0\Delta f}{h\nu}\right)^{\frac{1}{2}}$$

which is the noise from the unattenuated beam. Thus, the photon noise is independent of the absorption by intermediate gases.

Carbon Dioxide Density Fluctuations

The fluctuation in the number of molecules in a volume which on the average contains N molecules is $N^{\frac{1}{2}}$. There are on the average about 10^{15} carbon dioxide molecules in the laser beam at ambient pressure. The fluctuation is 3×10^{7} or 1 part in 30 million. Thus we could expect noise on the CO_2 absorption line of 3 parts in 10^{8} due to the density fluctuations of the CO_2. This, however, is much smaller than the noise which has been observed.

Heterodyne Detection of Fluorescence

Having ruled out noise due to the absorption process, we must conclude that the noise is due to heterodyne detection of radiation emitted from the carbon dioxide molecules. This radiation has been inelastically scattered by the molecules. If it had been elastically scattered, the bandwidth would be approximately $\bar{c}\alpha/\lambda$, where $\bar{c}$ = mean molecule velocity and α = beam convergence and this is approximately 1 MHz. Further, it would be independent of pressure.

The only difficulty with the suggestion that we are detecting the fluorescence signal is that it is about 100 times stronger than that calculated in Sec. 2.3. At this time no explanation can be given for this.

The relative strengths of the forward and backscattered signals were evaluated by placing a gas cell in the measuring volume of Fig. 8. Then as the pressure in the cell was pumped down, the linewidth of the backscattered signal would be reduced while the forward scattered signal, due to CO_2 near the detector, is unchanged. No change in the linewidth was observed, indicating that the signal was primarily due to forward scattering. This was confirmed by the fact that the sensor was most sensitive to CO_2 close to it.

Simplified Forward Scattering

From this stage on a simplified arrangement for the forward scattering was used. This employed only the single f/1 lens which collected the laser diode output and focused it onto the photodiode. The gas cell was placed immediately in front of the photodiode and could be evacuated.

Figure 9 shows a typical signal obtained as the laser is scanned through a CO_2 line. The upper trace is the photodiode output in the 3 - 20 MHz bandwidth. The "burst" of noise is clearly seen. The raw signal-to-noise ratio is about 17 dB. The lowest trace (inverted) is the crystal detector output and has a signal to noise ratio of about 50 dB. The laser power incident on the photodiode was approximately 100 μwatts.

Figures 11 and 12 show laser scans at a temperature of 18°K from 1.25 to 2.0 amps. These were performed at ambient pressure (760 mm Hg) and 47,000 ft (100 mm Hg). Strong lines are seen at 1.50, 1.60, 1.88, and 1.98 amps. These correspond to lines P(24), P(22), P(20), and P(18) (probably). The spacing between these lines is approximately 54 gHz from Table 2. There is also a very strong peak at 1.63 amps corresponding to the laser changing modes. At 1.50 amps only one mode could be measured during the calibration whereas at other currents, two modes were generally present. This may account for the signal at 1.5 amps being so strong. In fact, there is generally little correlation, between the strength of the absorption line and the "heterodyne" signal. This is probably because the "heterodyne" efficiency is a function of the spatial mode structure of the laser. This is most uniform when the laser is operating in a single mode. Indeed, a very strong signal was obtained when the laser operated at only one frequency.

The "P(22)" line at 1.60 amps increases in strength dramatically as the CO_2 pressure is reduced. This effect was repeatable and not due to a drift in the laser. The heterodyne signal strength is proportional to

$$gk \exp(-kL) \frac{\Delta F}{\Delta n}$$

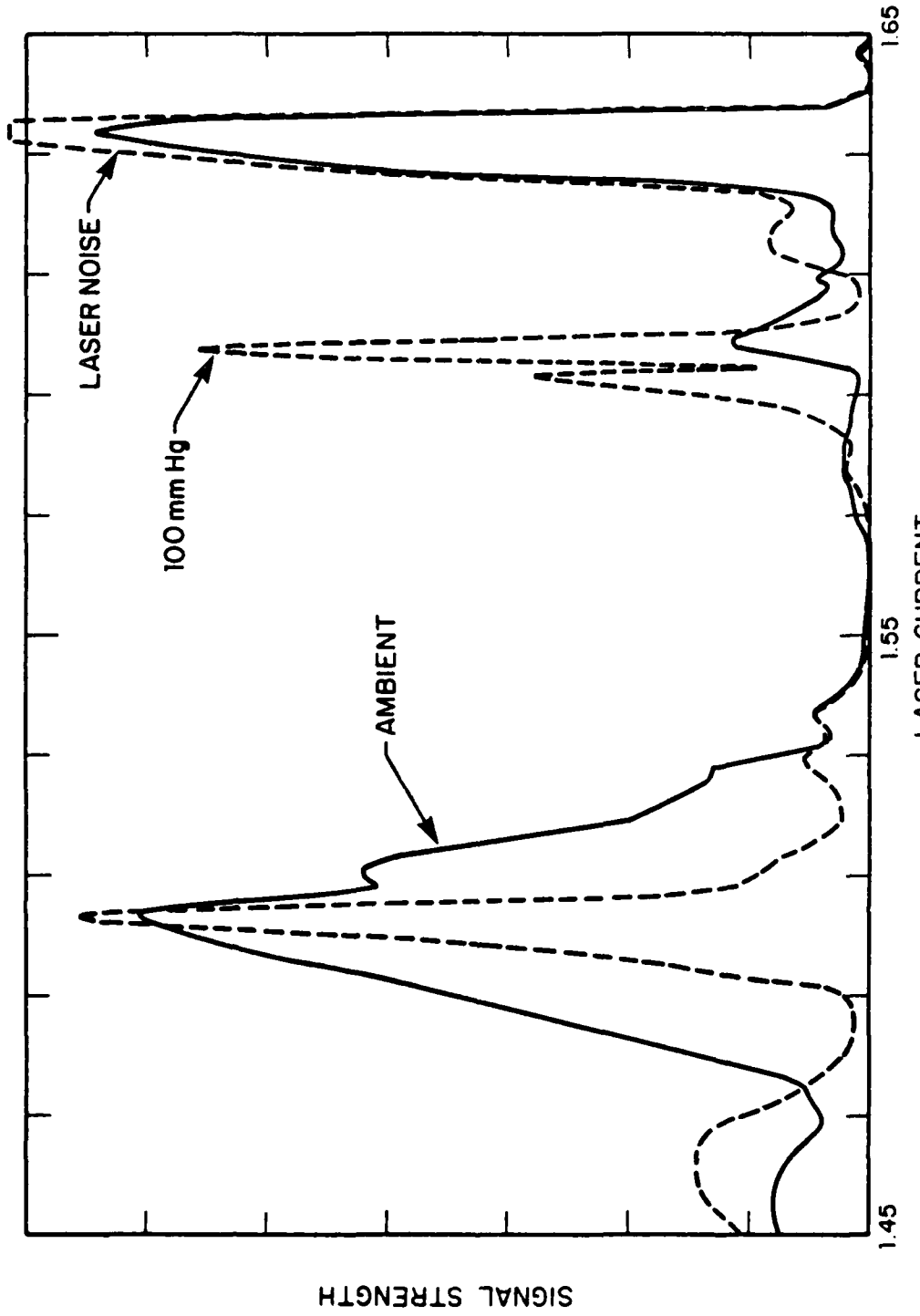

FIG. 11. SIGNAL FOR LASER AT 18°K, 1.45 - 1.65 AMP.

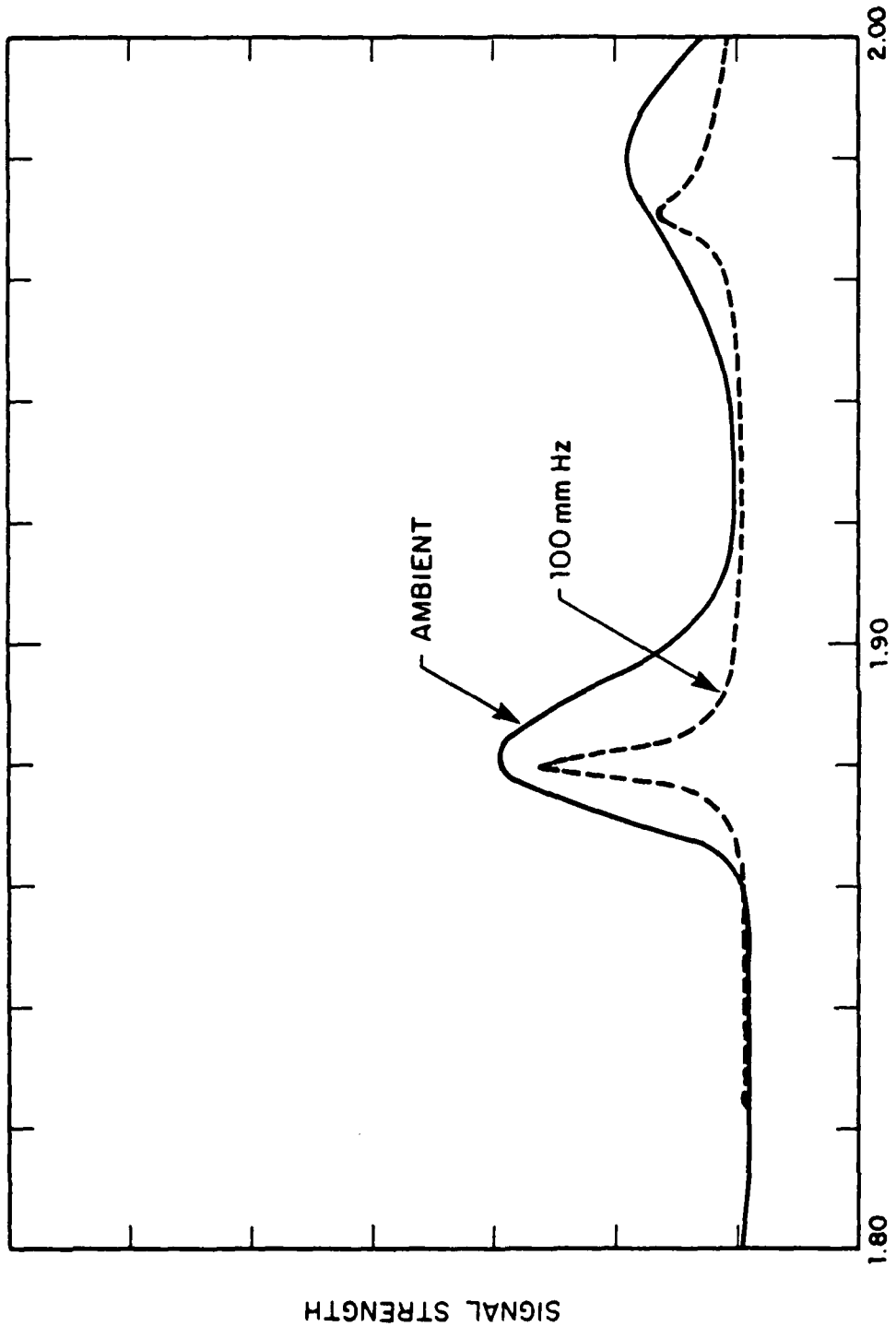

FIG. 12. SIGNAL FOR LASER AT 18°k, 1.80 - 2.00 AMPS.

where g = scattering efficiency $\alpha(\text{pressure})^{-1}$

k = absorption coefficient α pressure

ΔF = detector bandwidth

Δn = natural linewidth α pressure .

Thus,

$$\text{Signal} \alpha p^{-1} \exp(-p)$$

where p = pressure.

Thus the signal will increase as the pressure is decreased.

The reason not all the lines increase in strength as the signal is reduced is probably due to "saturation" of the strong absorption lines and only the weaker lines increase.

It will be noticed from Figs. 11 and 12 that the scan at 100 mm Hg produces substantially narrower lines than does the scan at ambient pressure (760 min). The scan rate of the laser is approximately 50 GHz/amp and this makes the linewidths approximately 10 GHz and 2 GHz, respectively. This is substantially greater than the 3 GHz and 0.5 GHz expected. However, this is probably due to the strong absorption of these lines which "saturates" the center and makes them appear wider than they really are.

4.3 Problems of the Fluorescence Measurement

1. Signal

As has been described above, extreme difficulties have been encountered in attempting to measure the fluorescence of atmospheric carbon dioxide. These difficulties have arisen primarily from:

a. The low level of the signal involved

b. interference from atmospheric carbon dioxide in the interferometer.

The signal is very weak and even if our detector has enough sensitivity, we would not see the signal because of the forward scattered signal from other carbon dioxide in the interferometer would mask it. This problem might be temporarily solved by using Nitrous Oxide (N_2O) or $C^{13}O_2$ for the fluroescence instead of $C^{12}O_2$. Nitrous oxide has a band centered at 4.57μ and $C^{13}O_2$ a band centered at 4.38μ compared with $C^{12}O_2$ a band centered at 4.26μ. Typically the R branch of $C^{12}O_2$ will overlap the P branch of $C^{13}O_2$ and thus a diode laser which can measure one can measure the other. Further, since the frequencies are not identical, they can be distinguished. Finally, only 1% of natural carbon dioxide contains C^{13} and hence interference from natural CO_2 will be small. This technique should then distinguish between the fluorescence of the $C^{13}O_2$ in a sample cell and forward scattering of $C^{12}O_2$ in the atmosphere. However, it is not a practical solution since $C^{13}O_2$ is rare in the atmosphere and if it were not, it would cause interference.

By comparison with the back-scattered signal, the absorption signal is very, very strong. The absorption could be used by placing a solid object in the flow and reflecting the radiation from the diode laser from it. This has been done, using a wire several feet from the laser. the scattered light is collected and focussed onto a photo-detector. Indeed a very strong signal was obtained. The problems with this technique are two-fold:

1. It requires something to be placed in the flow.
2. It does not localize the measurement but measures an average over the whole region through which the radiation has passed.

An alternative technique is to look at the absorption of infra-red radiation from an external source. If the sun were used, then the technique would only work in daytime and could not measure altitude since it would be averaging overall altitudes above the aircraft.

Thus this interference appears to be a very major problem for any practical aircraft system.

5. CONCLUSIONS

Generally the attempts to measure fluorescence from atmospheric carbon dioxide at infra-red wavelengths have been unsuccesful. There is some evidence of forward inelastic scattering in the forward direction. However, we have never seen any scattering in any other direction, but this may be due to interference from forward scattering produced by atmospheric carbon dioxide. This interference could be solved by using $C^{13}O_2$ as a fluorescing medium, but this would not be a practical solution.

The reason that the fluorescence is so difficult to detect is due primarily to the strength of competing mechanisms (collision with nitrogen and other carbon dioxide molecules) and the low power of the solid state diode laser (10^{-4} watts). These give signals levels low enough that sophisticated signal processing schemes have to be used.

The complexity and reliability of the laser diode system still leave much to be desired. It is difficult to envisage such a large and bulky system being installed on small high performance aircraft. The diodes themselves are unreliable, having finite shelf lives and degrading with uses. These problems may well be solved in time, but they have a long way to go.

The general conclusion must be that there must be a simpler, less exotic method for measuring air data. It was stated in the introduction that the problem with a pitot/static system is the measurement of the static pressure, not the total head

pressure. The pitot head gives very reliable results. It is the static port or ports that are so sensitive to position on the aircraft and to aircraft maneuvers. Therefore, what is needed is a better method for measuring the static pressure.

NASA is attempting to achieve this with their "Shuttle Entry Air Data System" (SEADS). This consists of 20 pressure taps around the nose of the shuttle and combines the pressure readings (with the aid of a computer) to give the air data. The problem with this technique is that it is very dependent on the shape of the aircraft nose and requires very extensive calibration, which then would have to be repeated for a different nose shape. However, the technique does give very reliable results and all the air data required, with only a modest degree of complexity.

A possible solution for aircraft application is to use a wing-tip mounted probe with, for example, five independent pressure ports. The tip of the probe would be a well defined shape, for example hemi-spherical and the ports could correspond to front, top, bottom, left and right. No one port would give the static pressure, but by ratioing the side ports with the front port, the total and static pressures can be computed. This would require an air-data computer, but so do present systems. It would also yield airspeed, altitude, and angles of attack and sideslip.

In conclusion then, a Laser Doppler Airspeed and Altitude Sensor is probably not the best way for the Air Force to proceed. Rather, sophisticated adaptions of the pitot-static tube should be considered, with multiple independent pressure ports.

REFERENCES

1. Bauer, E. and E.R. Reiter, "The Natural Stratosphere of 1974," Climatic Impact Assessment Program Report of Findings, DOT-TST-75-50. 1974.

2. Cheo, P.K., "Relaxation of CO_2 Laser Levels by Collision with Foreign Gases," *J. Quant Electron*, QE-4, p. 537. 1968.

3. Kildal, H. and R.L. Byer, "Comparison of Laser Methods for the Remote Detection of Atmospheric Pollutants," *Proc. IEEE*, 59, p. 1644. 1971.

4. Melngailis, I. and A. Mooradian, "Tunable Semiconductor Diode Lasers and Applicasocpy, Addison-Wesley, Reading, MA. 1975.

5. Munoz, R., H.W. Mocker and L. Koehler, "An Airborne Laser Doppler Velocimeter," *Applied Optics*, 13, p. 2890. 1974.

6. Seguin, J.N. and A.I. Carswell, "Fluorescence and Gain Measurements in a CO_2 TEA Amplifier," *J. Quant. Electron*, QE-8, p. 595. 1972.

7. Herzberg, G., *Molecular Spectra and Molecular Structure. II Infra-red and Raman Spectra of Polyatomic Molecules*. Van Nostrand (New York) 1945.

8. *Principles of Optics*, M. Born and E. Wolf, Pergamon Press, (4th Edition, 1970).

9. *Quantum Electronics*, A. Yariv, Wiley (2nd Edition, 1975).

BIBLIOGRAPHY

1. W.H. Louisell, A. Yariv, and A.E. Siegman (1961). Quantum Fluctuations and Noise in Parametric Processes I, *Physical Review* 124, pp. 1646-1654.

2. S.E. Harris, M.K. Oshman, and R.L. Byer (1967). Observation of Tunable Optical Parametric Fluorescence, *Physical Review Letters* 18, pp. 732-734.

BIBLIOGRAPHY (Cont.)

5. D. Magde and H. Mahr (1967). Study in Ammonium Dihydrogen Phosphate of Spontaneous Parametric Interaction Tunable from 4400 to 16,000 Å, *Physical Review Letters* 18, pp. 905-907.

6. T.G. Giallorenzi and C.L. Tang (1968). Quantum Theory of Spontaneous Parametric Scattering of Intense Light, *Physical Review* 166, pp. 225-233.

7. R.L. Byer and S.E. Harris (1968). Power and Bandwidth of Spontaneous Parametric Emission, *Physical Review* 168, pp. 1064-1068.

8. D.A. Kleinman (1968). Theory of Optical Parametric Noise, *Physical Review* 174, pp. 1027-1041.

9. A. Hordvik, H.R. Schlossberg, and C.M. Stickley (1971). Spontaneous Parametric Fluorenscence of Light in Proustite, *Applied Physics Letters* 18, pp. 448-450.

10. J. Falk, J.M. Yarborough, and E.O. Ammann (1971). Internal Optical Parametric Oscillation, *J. Quantum Electronics* QE-7, pp. 359-369.

11. J.E. Pearson, A. Yariv, and U. Daniel (1973). Observations of Parametric Fluorescence and Oscillation in the Infrared, *Applied Optics* 12, pp. 1168-1171.

APPENDIX A: SOURCE OF FLUORESCENCE SIGNAL

A possible source of the observed forward fluorescence signal is spontaneous parametric fluorescence. This nonlinear phenomenon gives a signal that is linearly proportional to the input power. Further, the radiation is emitted within a narrow bandwidth in the forward direction. The exact mechanism for the nonlinearity has not yet been identified.

A.1 Anomalous Dispersion

From Born and Wolf (1970, p. 92), the refractive index n near a resonance at a frequency ω_0 can be represented as

$$\frac{n^2 - 1}{n^2 + 2} = \frac{4\pi Ne^2}{3[m(\omega_0^2-\omega^2)-i\omega g]} \quad ,$$

where N, e, and m are the number per unit volume, the charge and mass of the electrons. Now for a gas $n \approx 1$ and thus $n^2 + 2 \approx 3$. Further, for $\omega = \omega_0 + \delta\omega$, where $\delta\omega$ is small

$$n^2 - 1 = \frac{4\pi Ne^2/\omega}{2m\delta\omega - ig} \quad .$$

Now, if the peak absorption per unit length = β and the linewidth is $\Delta\omega$, we can rewrite the above expression as

$$n^2 - 1 = \frac{2\beta/k}{2\delta\omega/\Delta\omega - i} \quad ,$$

where k is the wavenumber of the radiation. Further, if $n - 1 = \delta n$

$$\delta n = \frac{\beta c}{2\omega\delta\omega/\Delta\omega - i\omega}$$

and

$$\frac{dn}{i\omega} = \frac{2\omega\beta/\Delta\omega}{(2\omega\delta\omega/\Delta\omega - i\omega)^2} \quad .$$

When $\delta\omega = 0$

$$\left(\frac{dn}{d\omega}\right)_{min} \approx - \frac{2\beta c}{\omega\Delta\omega} \quad .$$

Now

$$\frac{dk}{d\omega} = \frac{n}{c} + \frac{\omega}{c}\frac{dn}{d\omega}$$

$$\left(\frac{dk}{d\omega}\right)_{min} = \frac{n}{c} - \frac{2\beta}{\Delta\omega} \quad ,$$

and this is the reciprocal of the group velocity. Now, if $2\beta/\Delta\omega$ is large enough, the group velocity can become infinite or even negative. However, under these conditions it no longer corresponds to the speed of transfer of energy, and thus causality is not violated.

The region of the absorption spectrum, where the group velocity is greater than the phase velocity, is referred to as anomalous dispersion.

Typical values for atmospheric carbon dioxide are $\beta = 5m^{-1}$ and $\Delta\omega = 4 \times 10^9$. Thus, $2\beta/\Delta\omega = (4\times10^8)^{-1}$ sec/m, which

is comparable with the reciprocal of the speed of light. At low pressures when $\Delta\omega = 2 \times 10^8$, β need only be 0.3 m^{-1} for the group velocity to become infinite.

An infinite group velocity means that waves of different frequencies have the same wavenumber, that is they are phase-matched. This means that, given a nonlinear mechanism, there is the possibility of frequency conversion, and this would take place over a bandwidth comparable to the resonance bandwidth.

A.2 Spontaneous Parametric Fluorescence

This phenomenon was first observed in the late 1960s. When a monochromatic plane wave propagates through a nonlinear medium, two other waves of lower frequencies are generated. The theory of this phenomenon is given by Yariv (1975). Parametric fluorescence is unusual among nonlinear effects in that the fraction of power that is converted from the initial pump beam into the fluorescent beam is independent of the intensity of the pump beam. It depends only on the nonlinear coefficient of the material and the distance that the pump beam travels through the medium. The fluorescence only takes place, in this case, in the forward direction, because that is the direction in which the phases are matched.

Yariv (1975) quotes the fraction of power P_2, which is changed in frequency as

$$\frac{P_2}{P_3} = \frac{\pi K \ell \theta^2}{|b|} \quad ,$$

with a bandwidth

$$\Delta\omega_2 = \frac{a\theta^2\ell - 2\pi}{b\ell} \quad ,$$

where K is a nonlinear interaction coefficient, θ the collection angle, ℓ the interaction length,

$$b = \left(\frac{dk_2}{d\omega_2}\right)_{\omega_{20}} - \left(\frac{dk_1}{d\omega_1}\right)_{\omega_{10}}$$

where ω_{20} and ω_{10} are the frequencies measured in the direction of the initial wave P_3, and $a = k_2k_3/2k_1$. In our case, $k_2 \approx k_3 \approx 1.5 \times 10^6 m^{-1}$ and $k_1 \approx 10\ m^{-1}$. Hence, $a \approx 10^{11} m^{-1}$ and

$$\Delta\omega_2 \approx a\theta^2/b \quad ,$$

and the power per unit bandwidth

$$\frac{P_2}{P_3\Delta\omega_2} = \frac{\pi K\ell}{a} \quad ,$$

or

$$\frac{P_2}{P_3} \approx 0.0006\, K\ell \text{ on a 20 MHz bandwidth.}$$

Note that although this is a nonlinear effect, the fluorescence is *linearly* related to the input power.

The value of K is given by

$$K = \frac{hk_1k_2^4}{(2\pi)^3} \frac{n_2}{n_1n_3} \frac{d^2}{\epsilon_0^3} \quad ,$$

where h is Plancks' constant, n_1, n_2, and n_3 are the refractive indices ≈ 1, ε_0 is the electric permitivity of free space, and d is the nonlinear part of the electric permitivity in the expression

$$P = \chi \varepsilon_0 + dE^2 + \ldots$$

where P is the polarisability, χ is the electric susceptibility, and E is the electric field. In general, P and E will be vectors and d will be a tensor, but we can ignore this in a gas. Then

$$K = 2.5 \times 10^{22} d^2 \text{ MKS} \quad .$$

Experimentally, values of $P_2/P_3 = 10^{-6}$ have been observed for a value of $\ell = 0.15$ m. This would require a value of $K = 10^{-12} m^{-2} sec^{-1}$, or a value of $d = 10^{-11}$ MKS.

This value of d is however very large compared with that generally found in solids. There the value is typically 0.3×10^{-22} MKS ($Li\ NbO_3$).

A.3 Nonlinearity Due to Saturation

The dielectric constant ε is given by

$$\varepsilon = 1 + \chi \quad .$$

For carbon dioxide $\chi \approx 10^{-3}$.
Let us suppose that there is an incident wave with a flux W watts/m^2, then

$$\varepsilon^2 E^2 = W z_0 \quad (\text{volts/m})^2 \ ,$$

where z_0 = impedance of free space = 377 ohm. Typical power densities in the experiments performed are around 100 watts/m^2 and, therefore,

$$E \approx 200 \text{ volts/m} \quad .$$

By any standard, this is not a strong field. However, because carbon dioxide is such a strong absorber, even this weak field can produce a significant nonlinearity.

Let us suppose that there are N carbon dioxide molecules per unit volume, each with an absorption cross-section of σ, for photons with a frequency ω.

Absorption per unit distance = N

Number of excited molecules/unit volume/unit time = $\frac{WN\sigma}{h\omega}$

Number of excited molecules/unit volume = $\frac{WN\sigma\tau}{h\omega}$

where τ = lifetime of excited molecule

Fraction of molecules that are excited = $\frac{W\sigma\tau}{h\omega}$

$$= \frac{\sigma\tau E^2}{h\omega z_0} \quad .$$

Now, the electric susceptibility is proportional to the number of molecules per unit volume. Hence,

$$\chi = \chi_0\left(1 - \frac{\sigma\tau E^2}{h\omega z_0}\right) \quad .$$

Taking $\sigma = 10^{-21}$ m^2, $\tau = 10^{-5}$ sec,

$$\chi = \chi_0(1-7\times10^{-10}E^2) \quad .$$

Thus, for a field of 200 volts/m, the susceptibility is reduced by a factor of 3×10^{-5}.

APPENDIX B: SIGNAL PROCESSING

A signal processing scheme is presented here for the measurement of the airspeed and altitude from the laser Doppler sensor in real time. The processing is based on computing the first and second moments of a cross-correlation function. This can be done with currently available A/D converters, a microprocessor, and very large-scale integrated (VLSI) multiplier and accumulator. The expected performance and implementation are discussed here. Given a 30-dB peak signal-to-noise ratio, an accuracy of 1 ft/sec in velocity and 500 ft at sea level in altitude can be expected.

B.1 Laser Airspeed Sensor Signal Analysis

The signal from the laser airspeed sensor consists of two channels: one from a reference cell and one from the air outside the aircraft. We shall call these the reference and signal channels. As the laser is scanned in frequency, so the signal in the detector varies. At low altitudes, the profile is Lorenztian (damped oscillator), which is determined by the pressure broadening. At high altitudes, where the profile is determined by Doppler motion, the profile is Gaussian. At intermediate altitudes, the envelope is the convolution of the two (Voight profile). What is desired here is a means of measuring the shift and width of the profiles, on the two channels, which is quick to perform (less than 100 msec), is insensitive to the exact form of the line profile, and enhances the signal-to-noise ratio (and, hence, the accuracy).

The form of signal processing described here is thought to meet these criteria. The principle is to compute the cross-correlation function between the two channels and then take the

first and second moments of this function. The first moment is related to the Doppler shift and the second moment to the line width.

Let us describe the reference channel by its photocurrent

$$I_R = I_R(f-f_0,\sigma_R)$$

and the signal photocurrent by

$$I_S = I_S(f-f_0-f_D,\sigma_S) \quad ,$$

where f_D is the Doppler shift. Now, the laser scans the frequency as a linear function of time. Therefore, we can substitute time (t) for frequency (f). The laser scan lasts for a time T and is digitized into N samples. The sample rate is $N/T = 1/\tau$. The 2N samples are stored in two memories. The two memories are multiplied and added together to give the first value of the cross-correlation function. One is then shifted by one sample period (τ) and again they are multiplied and added. This is repeated for all values of τ from -T to +T. This process of computation is lengthy but is often employed in signal processing. Accordingly, a very high-speed integrated circuit has been developed by TRW for this purpose. Each multiplication and addition takes only 70 nsec. However, we require a total of $2N^2$ operations. For N = 128, this would take a little over 2 msec to perform, which is very rapid indeed.

This normalized cross-correlation function is

$$C_{RS} = \frac{\int_0^T I_R(t-t_0,\sigma_R)\ I_S(t-t_0-t_D+\tau,\sigma_S)\ dt}{\int_0^T I_R(t-t_0,\sigma_R)\ I_S(t-t_0-t_D,\sigma_S)\ dt} \quad .$$

If we substitute $\tau' = \tau - t_D$, we see that this is the cross correlation of I_S and I_R without any Doppler shift, and then shifted by the Doppler shift. Let us then calculate the first moment of C_{RS},

$$M' = \frac{\int \tau C_{RS}(\tau - t_D)\, d\tau}{\int C_{RS}(\tau - t_D)\, d\tau}$$

$$= \left[\int (\tau - t_D)\, C_{RS}(\tau - t_D)\, d(\tau - t_D) / \int C_{RS}(\tau - t_D)\, d\tau\right] + t_D \quad .$$

Now, if the cross-correlation function is symmetric about t_D, the first term is zero and the second is equal to the time delay. Thus, $M' = t_D$.

The second moment,

$$M'' = \frac{\int \tau^2 C_{RS}(\tau - t_D)\, d\tau}{\int C_{RS}(\tau - t_D)\, d\tau}$$

$$= \frac{\int (\tau - t_D)\, C_{RR}(\tau - t_D)\, d(\tau - t_D)}{\int C_{RS}(\tau - t_D)\, d(\tau - t_D)}$$

$$+ 2t_D \frac{\int (\tau - t_D) C_{RS}(\tau - t_D)\, d(\tau - t_D)}{\int C_{RS}(\tau - t_D)\, d(\tau - t_D)} + t_D^2 \quad .$$

The first term is the second moment of the unshifted profile, which we call σ^2, and the second term is zero for a cross-correlation function symmetric about t_D. Thus, $M'' = \sigma^2 + t_D^2$.

B.2 Noise Calculation

Let us suppose that the signals from the reference and signal sensors have a noise power of $\overline{n^2}$. The noise of the two channels is thermal in origin and therefore is uncorrelated. However, because of the finite bandwidth of the noise, it does have some correlation in time. Let us call the value of the noise autocorrelation $G(\tau) = G(-\tau)$ at a time delay τ. Further, we shall presume that the noise bandwidth is sufficient that $G(\tau)$ is small and $G(2\tau)$ can be ignored.

When we compute the correlation function of the signal, we have N statistical independent multiplications of the noise and 2N multiplications with a correlation of $G(\tau)$. The result is a noise contribution of $\overline{n^2}\,[1+2G(\tau)]N^{\frac{1}{2}}$. This compares with the cross-correlation function of $N\bar{I}_R\bar{I}_S C_{RS}$, where the overbar denotes the time average. Thus, the normalized value of the noise is

$$= \frac{\overline{n^2}[1+2G(\tau)]}{N^{\frac{1}{2}}\bar{I}_R\bar{I}_S} \quad .$$

The first moment of this is

$$= \frac{\overline{n^2}T[1+2G(\tau)]}{2N\bar{I}_R\bar{I}_S}$$

$$= \overline{n^2}[1+2G(\tau)]/2I_RI_S \quad .$$

This is the average noise-to-signal ratio of the inputs times the sample time, times $[1+2G(\tau)]$ and divided by two. Similarly, the second moment of the noise is

$$= \frac{\overline{n^2}\tau^2[1+2G(\tau)]}{2N\bar{I}_R\bar{I}_S}$$

$$= \overline{n^2}\tau\tau[1+2G(\tau)]/2\bar{I}_R\bar{I}_S \quad .$$

Let us take a typical value for the signal-to-noise power ratio of 20 dB and N = 128 samples per scan. Then,

First moment noise ≈ 0.005 τ

Second moment noise ≈ 0.64 τ^2 .

[This assumes $G(\tau)$ is small.] Thus, the error in the first moment is very small, but it is much larger in the second moment. However, if the width of the cross-correlation function is 10 τ, the error is still only 0.64%.

The error reduces as N, the number of samples, increases. However, if this is done by sampling faster, eventually $G(\tau)$ becomes significant until no further benefit is obtained. Now,

$$G(\tau) = \exp(-2f_n\tau) \quad ,$$

where f_n = 3 dB down frequency for the noise. Thus, for a sampling frequency equal to f_n, $G(\tau)$ = 0.0018. Thus, in practice, $G(\tau)$ will only increase the error by about 0.36%, which is not significant.

B.3 Potential Problems with the Signal Processing

1. Asymmetry in Signal. If the reference and signal channels have the same envelope, but just shifted in time, then

we have seen that the cross-correlation function is the same as the autocorrelation function, but shifted relative to the origin. Now, any autocorrelation function of a real signal is symmetrical since the negative time delay is the same as swapping over the signals, which are identical. Thus, since the two channels are viewing the same physical phenomenon, the signals should be similar and produce a symmetrical correlation function. If this is not the case, then an error could be introduced.

3. *Signal Baseline.* In practice, the signal of interest is sitting on a baseline that contains no useful information. This baseline should be the same in both channels and accordingly will not contribute to the first moments of the autocorrelation function. However, it does contribute to the second moment and therefore must be removed. Since it is varying slowly, compared with the signal, it can be removed in several ways:

1. High pass analog filter
2. Direct computation
3. Differentiation of signal (analog or digital).

5. *Signal Distortion.* Errors will arise if the photosensor signal is distorted, for example, by using a limited bandwidth. However, these errors need not be large if the distortion is the *same* on both channels, i.e., the two line profiles are the same. This keeps the cross-correlation function symmetrical. Ideally, the two detectors should be matched with the same upper and lower cutoff frequencies. However, matching in *sensitivity* is not important since that only affects the absolute level of the signal and does not introduce any bias.

B.4 Overall Signal Processing Accuracy

The sweep time of the laser is T, and the signal is sampled N times in the sweep. The sampling frequency is then N/T, and we shall make this twice the bandwidth of the photo-sensors so that there is no sampling error. Now, the linewidths to be scanned vary from 0.2 to 4 GHz. Let us suppose then that we scan the laser through 12.8 GHz and take 128 samples. The signal is then sampled every 100 MHz. Now, if the peak signal-to-noise ratio is 5 dB, then the ratio of mean-square signal current to mean-square noise current is approximately

$$3 + 10 \log \left(\frac{\sigma}{12.5} \right) ,$$

where σ is the bandwidth of signal in Gigahertz. The signal current becomes less as the bandwidth becomes narrower, unless the sweep of the laser is reduced. This can be overcome by processing less of the scan at higher altitudes where the spectrum is narrower. This reduces both the sample time T and number of samples N, but leaves the sample frequency constant at N/T. Thus, suppose that the scan width is about 10 times the width of the spectrum. Then, we have an average signal-to-noise ratio of about 10 dB less than the peak signal-to-noise ratio. Thus, if we have a peak signal-to-noise ratio of 30 dB, we will have an average signal-to-noise ratio of 20 dB. The error in the velocity measurement is 0.005 × 100 MHz = 0.5 MHz, or about 1 m per sec. The error in the linewidth measurement is

$$\left(\frac{2}{N} \right)^{\frac{1}{2}} \times 10 \text{ MHz} ,$$

where N is the number of samples used ($\leq$ 128). At sea level, where N = 128, the error = 80 MHz or 30 mbar. This corresponds

to an uncertainty of 500 ft. This would be reduced to 160 ft if 256 samples were used instead of 128.

B.5 Implementation of Signal Processing

The signal processing would be implemented in two sections:

1. Hardwired logic to compute the correlation function
2. Programmed microprocessor to compute the first and second moments of the correlation function, convert to true airspeed and altitude, and conduct any corrections and calibrations required.

The correlation function is computed by hardwired logic because 32,768 multiplications and additions have to be performed and these would take too long with a microprocessor. A TRW TDC 1008 JM will perform an 8 × 8 bit multiplication and add the result into a 19 bit accumulator in a typical time of 70 nsec, with a maximum time between -55 and 125°C of 125 nsec. Thus, all the multiplications can be performed in a maximum of 4.096 sec. The computation of the first and second moments of the correlation function only require 256 multiplications and additions each and can be done at a more leisurely pace.

The schematic for the correlation function computer is shown in Fig. 1. It consists of a pair of 8 bit analog-to-digital converters, which sample the two photo-detectors. We shall call these inputs X and Y, although which is which is unimportant. There are three serial in/serial out shift register memories; an 8 × 256 bit X, an 8 × 128 bit Y, and a 16 × 256 bit OUT register. The data in the X and Y registers are multiplied and accumulated by a TDC 1008 JM interfaced

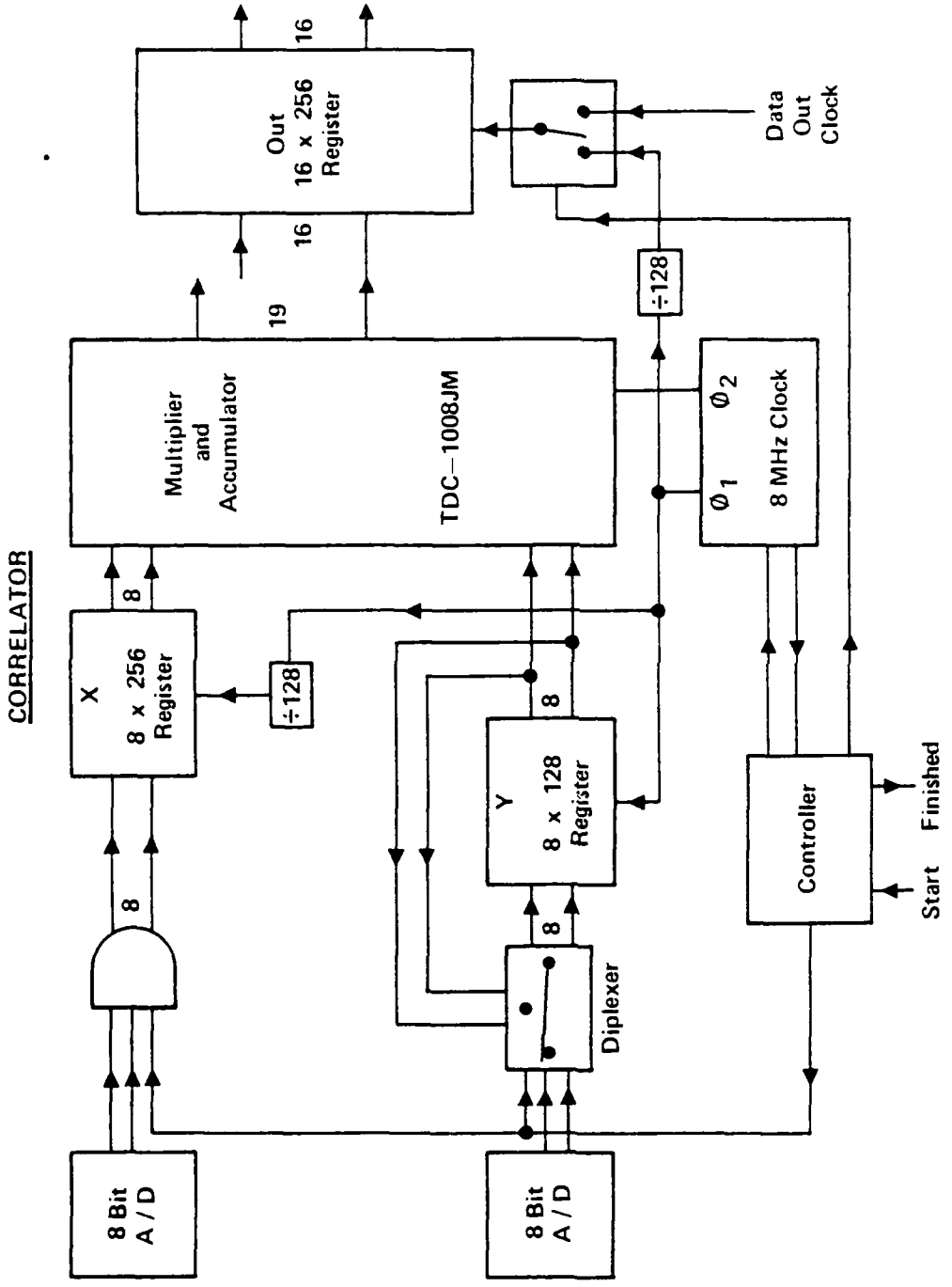

FIG. 1. SCHEMATIC FOR THE CORRELATION FUNCTION COMPUTER.

circuit and the 16 most significant bits are sent to the OUT register. The computation is sequenced by a controller, which can be a microprocessor. A biphase 5 MHz clock is used for the multiplier and registers.

In performing the computation, first 128, 8 bit words are loaded into the X and Y registers. This leaves the last 128 words of the X register empty and set to 0. These are required to produce the delay between the X and Y registers. The Y register is a recirculating memory. A diplexer on the input to the Y register selects data either from the A/D converter or the output of the Y register.

On each clock pulse, the first phase shifts the Y register one bit and on the second phase, the last words in the X and Y registers are multiplied and stored in the TDC 1008 JN. After 128 clock pulses, the Y register is back to its original condition. The accumulator result is then shifted to the OUT register and the X register is shifted one bit and the whole process is repeated again. The accumulator of the TDC 1008 JN has a 19 bit capacity, and we shall only use the 16 most significant bits. We shall suppose also that the gain of the A/D converters is such that the accumulator does not overflow.

This process is repeated 256 times until all the data have gone through the X register. The OUT register is then full. The first and second moments of the data in the OUT register are then computed and other calculations performed. The results are then transferred to the air data computer and the whole process is repeated.

The whole procedure for computing the correlation function takes 4.1 msec. However, half the multiplications are by 0 and therefore a more sophisticated controller might speed up the computation further. However, 4.1 msec may well be quite fast enough.

A high-speed correlator to compute the function for 128, 8 bit words in 4.1 msec can be constructed with the current state-of-the-art integrated circuits, using a VLSI multiplier/accumulator and 7K bits of registers. The whole processor can be mounted on one card and is compact enough for airborne applications.

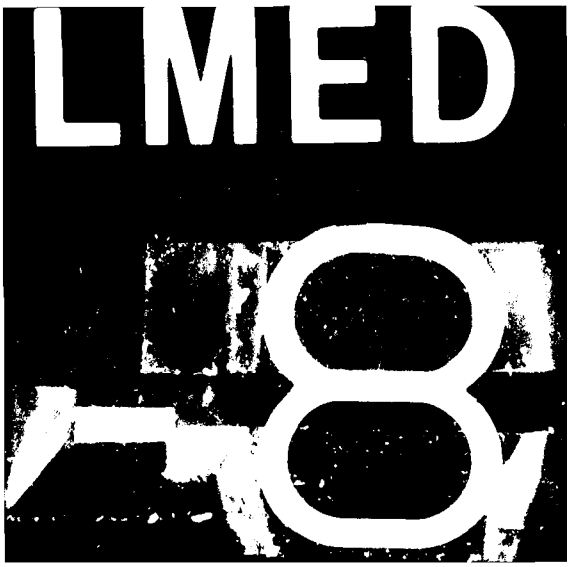
LMED
8